



**HAL**  
open science

# Targeted solvatochromic fluorescent probes for imaging lipid order in organelles under oxidative and mechanical stress

Dmytro I Danylchuk, Pierre-Henri Jouard, Andrey S Klymchenko

► **To cite this version:**

Dmytro I Danylchuk, Pierre-Henri Jouard, Andrey S Klymchenko. Targeted solvatochromic fluorescent probes for imaging lipid order in organelles under oxidative and mechanical stress. *Journal of the American Chemical Society*, 2021, 143 (2), pp.912-924. 10.1021/jacs.0c10972 . hal-03292160

**HAL Id: hal-03292160**

**<https://hal.science/hal-03292160v1>**

Submitted on 20 Jul 2021

**HAL** is a multi-disciplinary open access archive for the deposit and dissemination of scientific research documents, whether they are published or not. The documents may come from teaching and research institutions in France or abroad, or from public or private research centers.

L'archive ouverte pluridisciplinaire **HAL**, est destinée au dépôt et à la diffusion de documents scientifiques de niveau recherche, publiés ou non, émanant des établissements d'enseignement et de recherche français ou étrangers, des laboratoires publics ou privés.

# Targeted solvatochromic fluorescent probes for imaging lipid order in organelles under oxidative and mechanical stress

Dmytro I. Danylchuk,<sup>1</sup> Pierre-Henri Jouard,<sup>1</sup> Andrey S. Klymchenko<sup>1,\*</sup>

<sup>1</sup>Laboratoire de Bioimagerie et Pathologies, UMR 7021 CNRS, Université de Strasbourg, 74 route du Rhin, 67401, Illkirch, France

## ABSTRACT

Biomembranes constitute a basis for all compartments of live cells, and therefore monitoring their lipid organization is essential for understanding cell status and activity. However, sensing and imaging lipid organization specifically in different organelles of live cells remains challenging. Here, we designed an array of solvatochromic probes based on Nile Red bearing ligands for specific targeting of endoplasmic reticulum, mitochondria, lysosomes, Golgi apparatus, plasma membranes and lipid droplets. These polarity-sensitive probes detected variations in the lipid order by changing their emission maximum, as evidenced by fluorescence spectroscopy in model membranes. In colocalization microscopy experiments with reference organelle markers, they exhibited good organelle selectivity. Using two-color fluorescence microscopy, the new probes enabled imaging local polarity of organelles in live cells. To exclude the biased effect of the probe design on the sensitivity to membrane properties, we calibrated all probes in model membranes under the microscope, which enabled first quantitative description of lipid order in each organelle of interest. Cholesterol extraction/enrichment confirmed capacity of the probes to sense lipid order, revealing that organelles poor in cholesterol are particularly affected by its enrichment. The probes also revealed that oxidative and mechanical stresses produced changes in the local polarity and lipid order that were characteristic for each organelle, with mitochondria and lysosomes being particularly stress-sensitive. The new probes constitute a powerful toolbox for monitoring the response of the cells to physical and chemical stimuli at the level of membranes of individual organelles, which remains an underexplored direction in the cellular research.

## INTRODUCTION

Specific targeting and imaging of organelles in live cells attracted significant interest in recent years.<sup>1-8</sup> Possible strategies utilized to achieve organelle selectivity typically exploit biological or chemical methods by tethering fluorophores either to biomolecules, such as peptides, lipids and oligosaccharides, or to chemically designed moieties.<sup>1</sup> The organelle targeting is particularly interesting to monitor organization of lipids, which are building blocks for all live cell compartments, present either in form membrane bilayers<sup>9-10</sup> or spherical core-shell structures (lipid droplets, LDs).<sup>11</sup> Lipid organization in biomembranes is controlled by cholesterol (Chol) and sphingomyelin (SM), which are enriched in cell plasma membrane, but less abundant in the intracellular membranes.<sup>12-13</sup> These lipids are responsible for formation of liquid ordered (Lo) phase,<sup>14</sup> which plays a crucial role in formation of lipid microdomains.<sup>9-10,15</sup> Unsaturation degree of phospholipids is also of primary importance for biomembrane organization, as saturated lipids favor Lo and gel phases, while unsaturated lipids constitute liquid disordered (Ld) phase.<sup>10,16</sup> Lipid unsaturation is finely tuned by the cells to preserve lipid organization,<sup>17</sup> and the distribution of unsaturated lipids is uneven due to enzymes, such as desaturases, present in the endoplasmic reticulum (ER).<sup>18</sup> On the other hand, most of triglycerides, cholesterol esters are localized in LDs, a storage of energy and lipids, maintaining homeostasis of cells and protecting them from stress conditions.<sup>19</sup>

Environment-sensitive fluorophores such as molecular rotors, mechanosensitive and solvatochromic dyes enable monitoring lipid organization of cell organelles by detecting local viscosity, mechanical tension and polarity, respectively.<sup>20-21</sup> Molecular rotors, operating by excited-state planarization of dyes with high rotational freedom, were successfully used to monitor membrane viscosity especially using fluorescence lifetime imaging.<sup>20,22-23</sup> BODIPY molecular rotor bearing membrane-anchor moiety have been proposed for imaging microviscosity in cell plasma membranes.<sup>24</sup> Organelle-targeted molecular rotors have been also recently reported by using genetically-encoded protein tag (HaloTag), which are able to sense microviscosity in cytosol, nucleus, ER and mitochondria.<sup>25</sup> Mechanosensitive dyes based on ground-state planarization (flippers)<sup>26-27</sup> have recently emerged as powerful probes for membrane tension, parameter that also correlates with lipid order in biomembranes.<sup>28-29</sup> Their conjugates with organelle-targeting chemical groups enabled monitoring membrane-tension specifically in plasma membranes, mitochondria, ER and lysosomes.<sup>5</sup> Their reactive derivatives (HaloFlippers) for labelling HaloTag fused to membrane proteins have also been recently developed for probing biomembranes in any desired organelles of interest.<sup>30</sup>

Solvatochromic dyes, which are push-pull fluorophores undergoing excited state charge transfer, change their emission color in response to polarity. These dyes can report on the physical state of biomembranes<sup>31</sup> and its alterations during apoptosis,<sup>32-33</sup> starvation,<sup>34</sup> oxidative stress,<sup>34</sup> while also distinguishing normal and cancerous cells.<sup>35-36</sup> Owing to their sensitivity to membrane hydration, dielectric properties (polarity) and solvent relaxation, solvatochromic dyes are particularly suitable for probing lipid order.<sup>21,37-38</sup> Indeed, in tightly packed Lo phase, characterized by lower hydration, polarity and fluidity, they show blue shifted emission compared to Ld phase.<sup>31</sup> A variety of solvatochromic dyes have been applied for this purpose, which includes Laurdan,<sup>39</sup> styrylpyridinium dyes,<sup>40-41</sup> 3-hydroxyflavones,<sup>42</sup> Nile Red,<sup>43</sup> push-pull anthracene,<sup>44</sup> pyrenes,<sup>45-46</sup> and dioxaborine,<sup>34</sup> etc. Previously, the efforts were mainly focused on targeting cell plasma membranes with solvatochromic dyes by grafting both charged and lipophilic groups, as exemplified for Di-4-ANEPPDHQ,<sup>40</sup> C-Laurdan,<sup>47</sup> Pro12A,<sup>48</sup> F2N12S,<sup>33</sup> NR12S,<sup>43</sup> etc. However, imaging intracellular membranes with solvatochromic dyes emerged only in the recent years. Two approaches have been followed. The first one uses a non-specific lipophilic probe that redistributes in biomembranes of different organelles within the cell, thus allowing polarity and lipid order mapping irrespectively to a given organelle.<sup>34,45-46,49</sup> It revealed that the intracellular biomembranes are significantly more polar (less ordered)

than plasma membranes.<sup>46</sup> Second approach exploited specific targeting of solvatochromic dyes to organelle of interest,<sup>5,25,35-36,50-53</sup> including mitochondria<sup>32,50,54</sup> and ER.<sup>35</sup> However, these studies were focused on targeting one particular organelle. Specific targeting of different organelles using a family of probes based on the same solvatochromic dye would enable direct comparison of properties of organelles and their response to different stress conditions.

Nile Red, originally proposed as lipid droplet marker,<sup>55</sup> has a favorable position among existing solvatochromic dyes, because it combines high brightness, operation in the optimal (yellow-red) spectral region and good sensitivity to lipid order.<sup>43</sup> Due to its fluorogenic character it enabled spectrally resolved super-resolution (PAINT) imaging of lipid order.<sup>56-57</sup> Its functionalization with membrane anchor groups led to a family of probes, NR12S, NR12A and NR4A for ratiometric and spectral imaging of lipid order specifically in the plasma membranes.<sup>43,58</sup> In particular, functionalization of Nile Red at the amino end was found to improve dye photostability, which is crucial for advanced microscopy.<sup>58</sup> Therefore, we considered that functionalization of Nile Red with organelle targeting groups could yield a powerful toolbox for addressing polarity and lipid order in any desired organelle in live cells.

In the present work, we synthesized a family of Nile Red derivatives bearing chemical groups for specific targeting of organelles, such as mitochondria, ER, Golgi apparatus, lysosomes and LDs, in addition to plasma membranes. The new probes preserved sensitivity of Nile Red to lipid order in lipid membranes. Cellular studies confirmed their organelle-specific targeting. These probes revealed that each organelle is characterized by its unique polarity/lipid order profiles, which vary in different ways under oxidative and mechanical stress.

## RESULTS AND DISCUSSION

In order to obtain solvatochromic organelle-specific probes we conjugated Nile Red fluorophore with targeting moieties (Figure 1A). We have already reported plasma membrane targeting of Nile Red using alkyl sulfonate with dodecyl chain (probe NR12A).<sup>58</sup> Conjugation from amino end of Nile Red dye improved its performance compared to that using phenolic group,<sup>58</sup> therefore, we selected the amino-end conjugation strategy for all organelle-targeting probes. To target mitochondria, we used triphenylphosphonium,<sup>59</sup> which is known to accumulate in mitochondria by crossing the inner mitochondrial membrane driven by the transmembrane potential.<sup>1,5,60-61</sup> N-Alkylmorpholin moiety, owing to its reversible protonation at physiological pH, was used for lysosomes.<sup>1,5,52,62</sup> Propylchloride<sup>1,63</sup> and pentafluorophenyl<sup>5,35,60</sup> were used for targeting ER, whereas myristic acid – for targeting Golgi apparatus.<sup>64</sup> To improve affinity of Nile Red to lipid droplets we grafted it to two cyclohexyl moieties, which we earlier used in LDs-specific statomero-cyanines.<sup>65</sup> All probes were synthesized starting from previously reported<sup>58</sup> Nile Red derivative bearing carboxylic acid (NR-COOH). The products were obtained in moderate to good yields by an amide coupling with corresponding targeting ligands (Figure 1, see Figure S1 of the Supporting Information).

Owing to the lipophilic nature of the Nile Red moiety, the designed probes are expected to report the local polarity and lipid order in biomembranes of specific organelles by their characteristic emission wavelengths. Moreover, they are expected to sense cholesterol content in biomembranes of organelles, oxidative stress due to change in polarity of biomembranes caused by lipid peroxidation,<sup>34</sup> and

hyperosmotic shock due to altered lipid order in organelle membranes, associated with mechanical stress (Figure 1C).<sup>58,66</sup>

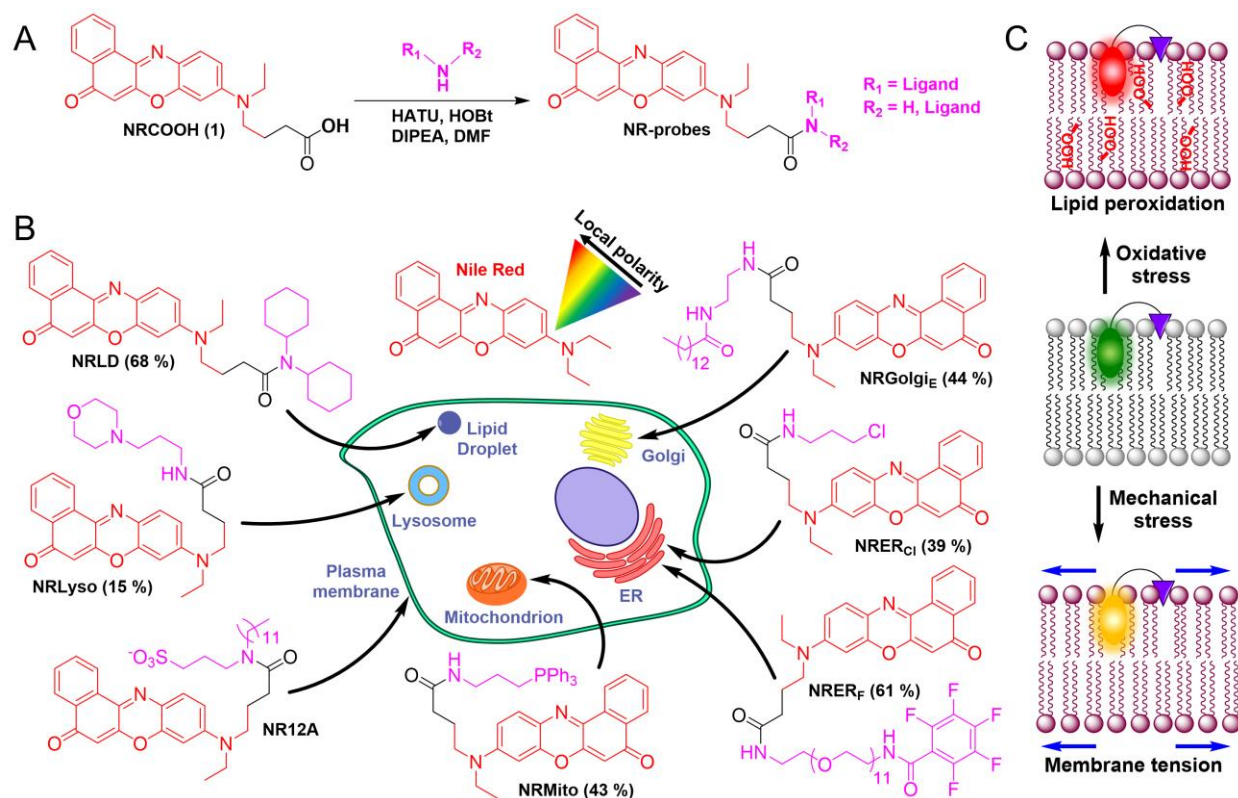


**Figure 1.** Organelle-targeted solvatochromic probes based on Nile Red. (A) General scheme of synthesis, (B) chemical structures (and the reaction yields) of the developed probes (NR12A was reported previously<sup>58</sup>). (C) Presentation of the color response of a solvatochromic probe to oxidative and mechanical stress in lipid membranes.

In organic solvents of different polarity all new probes showed high fluorescence quantum yields and the solvatochromic shifts with band position similar to that of parent Nile Red (Table 1, Table S1), which indicates that the fluorophore preserved its optical properties, including solvatochromism. Then, we studied the probes in large unilamellar vesicles (LUVs), which are model lipid membranes of different composition presenting Ld phase (1,2-dioleoyl-*sn*-glycero-3-phosphocholine, DOPC and DOPC/Chol) and Lo phase (SM/Chol). In DOPC LUVs, all probes showed fluorescence enhancement with good quantum yields compared to buffer, which was accompanied by a blue shifted emission around 640–650 nm (Table 1, Figure 2, Figure S2). These results suggest that all studied probes partition well into Ld phase, where they sense less polar environment compared to water. Further blue shift of the band was systematically observed in the presence of cholesterol, showing their sensitivity to dehydration produced by cholesterol, similarly Nile Red probes.<sup>31</sup> Much stronger effects were observed in SM/Chol LUVs, where emission band shifted to the blue by 40–60 nm vs DOPC LUVs, similarly to parent Nile Red, indicating that the probes preserved capacity to detect much less polar/hydrated environment of tightly packed Lo phase, in line with other solvatochromic dyes.<sup>21</sup> The exception was NRER<sub>F</sub>, which showed strong contribution of emission form the

buffer with a blue shifted shoulder corresponding to the Lo phase (Figure S2). The latter indicates that the probe is excluded from tightly packed Lo phase, probably due to the high bulkiness and/or polarity of its targeting moiety. Nevertheless, the blue shifted shoulder suggests that non-negligible fraction of the probe partitions into vesicles and identifies low-polar environment of the Lo phase. Overall, the new probes can bind lipid membranes and distinguish the Lo phase as much less polar compared to the Ld phase.

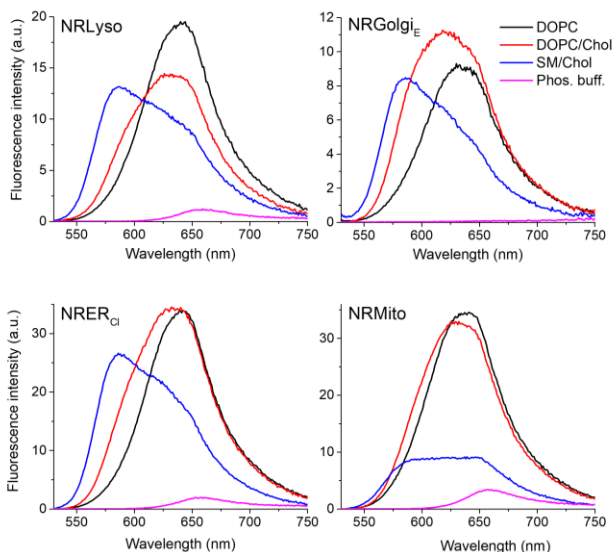


**Figure 2.** Fluorescence emission spectra of probes NRlyso, NRGolgi<sub>E</sub>, NRER<sub>Cl</sub>, NRMito in lipid vesicles (LUVs) of different composition. Probe concentration was 2  $\mu$ M. Total lipid concentration was 1 mM. Excitation wavelength was 520 nm.

**Table 1.** Fluorescence properties of probes in organic solvents and lipid vesicles of different composition.<sup>a</sup>

Solvent or medium		Probe							
		NRMito	NRLyso	NRER <sub>F</sub>	NRGolgi <sub>E</sub>	NRER <sub>C1</sub>	NRLD	NR12A <sup>b</sup>	Nile Red <sup>b</sup>
<b>DOPC</b>	$\lambda_{\max}$ em	641	640	647	630	639	645	641	639
	QY, %	43	36	34	21	38	61	51	55
<b>DOPC/Chol</b>	$\lambda_{\max}$ em	632	626	644	618	632	626	636	636
	QY, %	50	41	48	31	55	61	47	71
<b>SM/Chol</b>	$\lambda_{\max}$ em	639	587	653	586	586	582	592	589
	QY, %	24	40	21	28	56	47	39	52
<b>Phos. buff.</b>	$\lambda_{\max}$ em	660	659	654	736	653	743	648	666
	QY, %	6.9	5.8	9.5	0.4	6.5	0.33	0.36	4.2
<b>MeOH</b>	$\lambda_{\max}$ em	643	643	642	642	645	646	641	641
	QY, %	37	41	43	41	42	42	44	38
<b>Acetone</b>	$\lambda_{\max}$ em	612	584	615	615	613	615	619	615
	QY, %	59	58	74	77	86	74	70	70
<b>Dioxane</b>	$\lambda_{\max}$ em	602	580	591	586	584	584	602	585
	QY, %	74	53	78	78	75	78	70	74

<sup>a</sup> Probe concentration was 2  $\mu$ M. For liposomes, the total lipid concentration was 1 mM. <sup>b</sup> Data from a previous work.<sup>58</sup>

In order to evaluate the capacity of the probes to target a given organelle, we incubated them with live KB (Figures 3 and S3) and HeLa (Figure S4) cells together with corresponding organelle markers. Importantly, each new probe showed significant colocalization with corresponding commercial marker in both cell lines, having Pearson's correlation coefficient values in KB cells within the range from 0.89 to 0.96 (SI Table S2) (except NRGolgi<sub>E</sub> showing a bit lower values). Probe NRLyso in both cell lines exhibited even higher selectivity compared to commercial LysoTracker Green, which is clear from the observed lower background noise in the images (Figure 3E and S4E). Moreover, NRLD in HeLa cells, showed higher selectivity towards lipid droplets compared to the parent Nile Red dye (Figure S4 G,H), which is probably because of much higher hydrophobicity and bulky nature of dicyclohexylamino group.

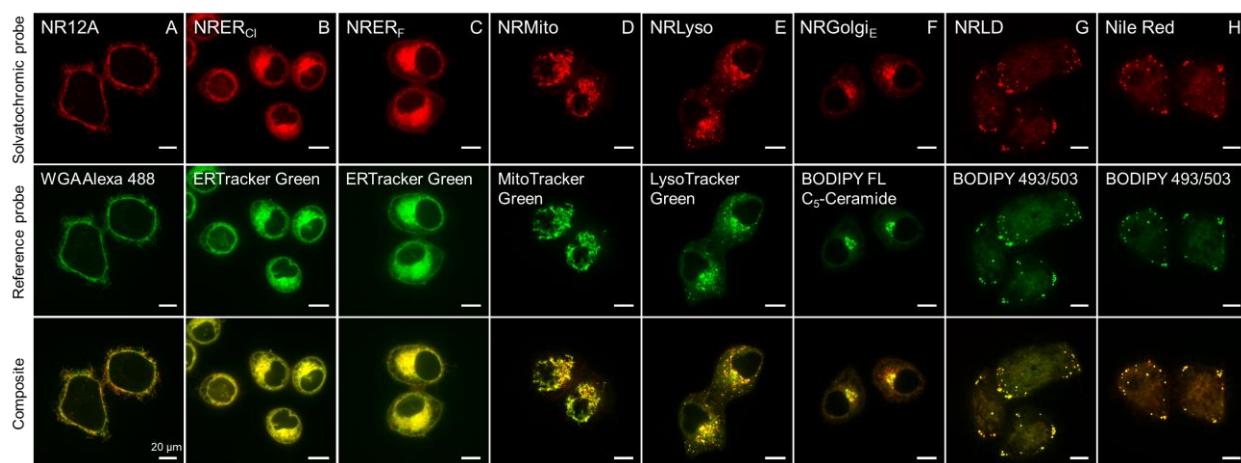


**Figure 3.** Colocalization of solvatochromic probes (in red) with commercial organelle probes (in green) in live KB cells. Solvatochromic probe concentration: 20 nM for NR12A; 50 nM for NRMito, NRLyso, NRLD, NRER<sub>C1</sub>; 200 nM for NRER<sub>F</sub>; 2.5 μM (in form of BSA complex) for NRGolgi<sub>E</sub>.

As the emission band position of Nile Red describes the local polarity and order of lipid structures, we analyzed this parameter by recording the short- and long-wavelength parts of the dye emission band below and above 600 nm and then constructed ratiometric images, in line with previously used methodology.<sup>43</sup> Before cellular analysis, each probe was calibrated under the microscope in the model lipid membranes (LUVs) presenting the Lo and Ld phases, which correspond to extreme examples of order and disorder in lipid membranes. In case of NRLD probe, Lo phase vesicles were replaced with sesame oil, which was expected to mimic non-polar environment in the oil core of LDs. Ratiometric fluorescence microscopy of LUVs (appeared as homogeneous signal, because individual vesicles cannot be resolved on this timescale) showed drastic difference in the pseudo-color (Figure 4A) of the probes when Ld and Lo phases were compared. Indeed, green/red fluorescence intensity ratio was systematically higher the Lo phase, which corresponded to the blue shift in the emission spectra observed by spectroscopy (Figure 2 and Figure S2). Then, we analyzed the distribution of the green/red intensity ratio in the images (Figure 4C) and further obtained an average ratio values (Figure 4D, Table S3), which allowed us to quantify the amplitude of probe ratiometric response to Ld-Lo phase change. Both the ratio value and its variation in response to the phase change were characteristic for each probe, in line with the spectroscopy data above. Having our calibration data for Ld and Lo phases, we performed the ratiometric imaging of live KB cells (Figure 4B, Figure S5). Strikingly, the pseudo-color showed dramatic variation in different organelles, which reflected strong differences in the green/red ratio (Figure 4C,D) and thus local polarity. Indeed, the observed orange pseudo-color in mitochondria and ER indicated the most polar microenvironment, whereas blue-violet dots for lipid droplets and blue-green plasma membranes reflected much lower local polarity (Figure 4B).

Local polarity detected by solvatochromic dyes reflects lipid order in biomembranes: the higher lipid order (and tighter lipid packing) the lower local polarity and hydration.<sup>31</sup> To interpret these local polarity variations in terms of lipid order, for each probe we compared the green/red ratio in cells with that in our calibration images of LUVs (Figure 4C,D). While the ratio values for the plasma membrane probes were close to those in Lo phase of LUVs, those for ER and Golgi (NRER<sub>F</sub> and NRGolgi<sub>E</sub>) were close to those in Ld phase. To quantitatively describe the effects, we introduce a lipid order parameter, LOP = (R-



$R_{DOPC}/(R_{SM/Chol}-R_{DOPC})$ , which approaches 0 and 1, when the green/red ratio (R) is close to that in Ld ( $R_{DOPC}$ ) and Lo ( $R_{SM/Chol}$ ) phase LUVs, respectively (Figure 4E). According to this analysis, the plasma membranes presented the highest level of lipid order, close to that of SM/Chol, in line with earlier works.<sup>42-43,49</sup> Intracellular, organelles displayed much lower LOP values, which decreased in the following order:  $NR_{Mito} \sim NR_{ER_{Cl}} > NR_{Liso} > NR_{Golgi_E} > NR_{ER_F}$ . The two probes, staining endoplasmic reticulum ( $NR_{ER_{Cl}}$  and  $NR_{ER_F}$ ), exhibited very different local lipid order, possibly due to much shallower insertion of  $NR_{ER_F}$  fluorophore inside ER membrane. In case of LDs, the LOP quantification was not applied, because the core shell structure of LDs is different from lipid bilayers. The green/red ratio value for LDs ( $NR_{LD}$ ) were close to those in sesame oil (Figure 4C), reflecting a non-polar environment in the oil core of LDs.

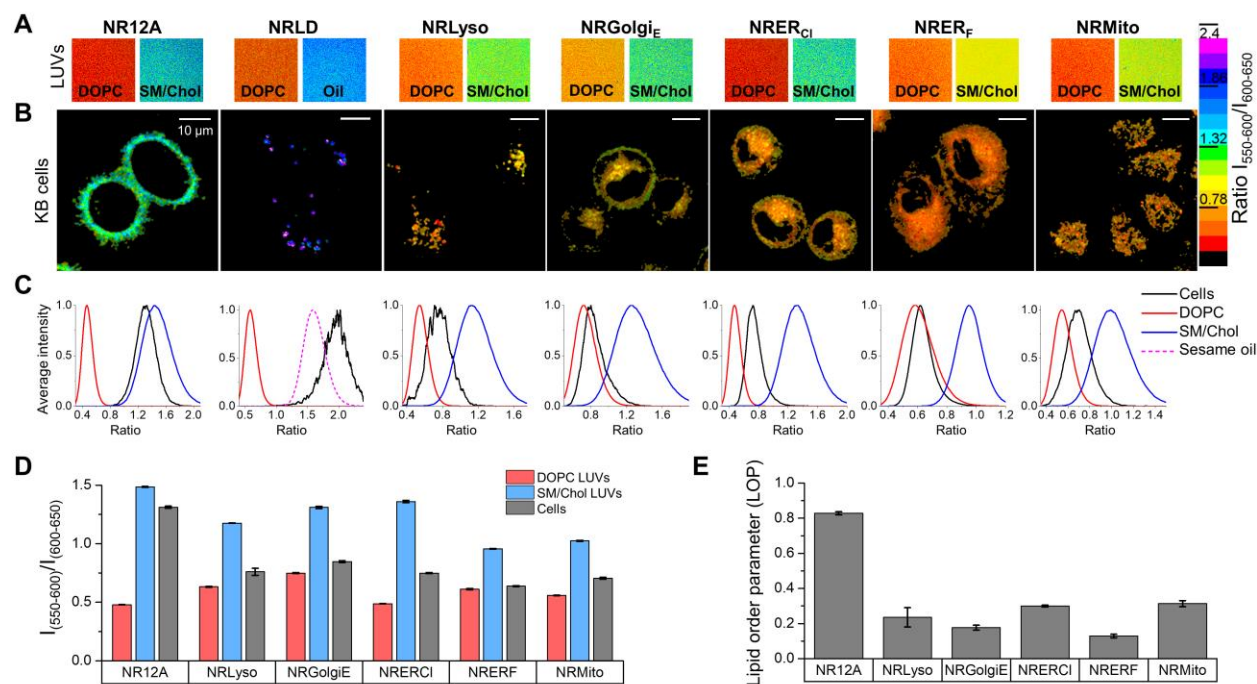


**Figure 4.** Solvatochromic organelle-specific probes reveal differences in polarity and lipid order within the organelles in KB cells. (A) Ratiometric confocal imaging of LUVs presenting Lo (DOPC) and Ld (SM/Chol) phases for calibration of the probes (in case of NRLD, sesame oil was used instead of the SM/Chol LUVs). Lipid and probe concentrations were 500 and 1  $\mu$ M, respectively. (B) Ratiometric confocal imaging of KB cells by the solvatochromic organelle probes. Probe concentration: 20 nM for NR12A; 50 nM for NRMito, NRLyso, NRLD, NRER<sub>Cl</sub>; 200 nM for NRER<sub>F</sub>; 5  $\mu$ M (in form of BSA-conjugate) for NRGolgi<sub>E</sub>. (C) Distribution histogram of the green/red fluorescence intensity ratio ( $I_{550-600}/I_{600-650}$ ) for corresponding probes in KB cells. (D) Weighted arithmetic mean values of the  $I_{550-600}/I_{600-650}$  ratio obtained from LUVs and cell imaging data (A,B). (E) Lipid order parameter (LOP) calculated from ratiometric images of organelle probes in KB cells and LUVs under various conditions.

Cholesterol is an essential component of biomembranes, distributing all over the cell.<sup>9,12-13</sup> Its excessive accumulation in cells is associated with variety of diseases, including atherosclerosis<sup>67</sup> and Niemann-Pick C1 disease.<sup>68</sup> On the other hand, cholesterol extraction by treating the cells with methyl- $\beta$ -cyclodextrin

(MBCD)<sup>69</sup> leads to an impaired signal transduction due to disruption of lipid microdomains.<sup>9-10</sup> We applied our new probes to study the effects of cholesterol extraction and enrichment on biomembranes in different organelles. Cholesterol extraction produced significant changes in the ratiometric images (Figures 5A and S6), corresponding to the decrease in the green/red ratio and the LOP values for all probes (Figures 5B and 6). Thus, our probes detect the increase in the local polarity associated with the loss of lipid order in all targeted organelles. This implies that the Nile Red fluorophore in all these probes is indeed inserted in the lipid membranes of corresponding organelles, which further validates our approach of organelle-specific lipid order sensing. Moreover, this result also confirms that cholesterol is distributed all over the cells and its removal affects local membrane properties in all studied organelles. Importantly, cholesterol enrichment using MBCD/Chol complex produced the opposite effect, although the effect varied within the organelles. The increase in the green/red ratio and corresponding LOP values was particularly strong in case of lysosomes and ER (Figure 6), initially characterized by low lipid order and relatively low cholesterol content according to the literature data.<sup>12</sup> Thus, our probes reveal that cholesterol enrichment affects mostly lipid order of the intracellular membranes with poor cholesterol content, in contrast to weakly affected plasma membranes, rich in cholesterol.

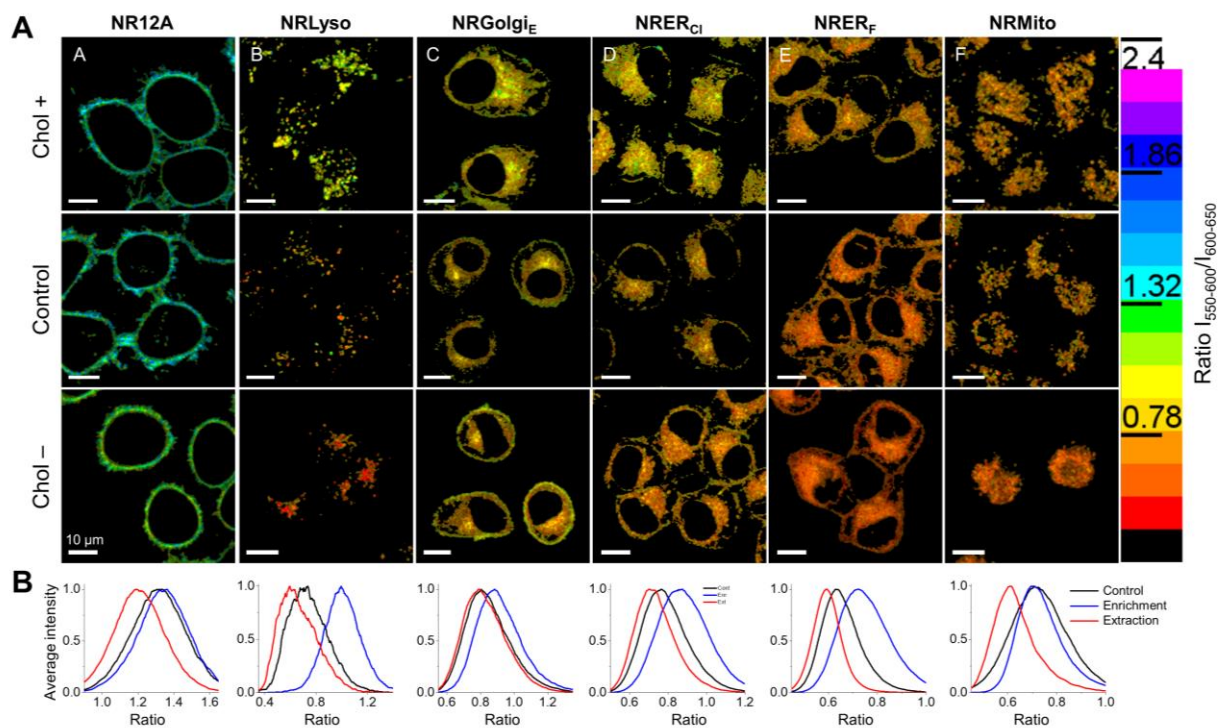


**Figure 5.** (A) Confocal ratiometric imaging of live KB cells with varied cholesterol content, using solvatochromic probes for organelles. Cholesterol enrichment (top panel) was produced by a saturated Chol:MBCD complex (3h at 37°C); cholesterol extraction (bottom panel) was produced by 5 mM MBCD (1h at 37°C). Probe concentration: 20 nM for NR12A; 50 nM for NRMito, NRLyso, NRLD, NRERCl; 200 nM for NRERF; 5 μM (in form of BSA-conjugate) for NRGolgiE. (B) Distribution histogram of the green/red fluorescence intensity ratio ( $I_{550-600}/I_{600-650}$ ) for corresponding probes in KB cells.

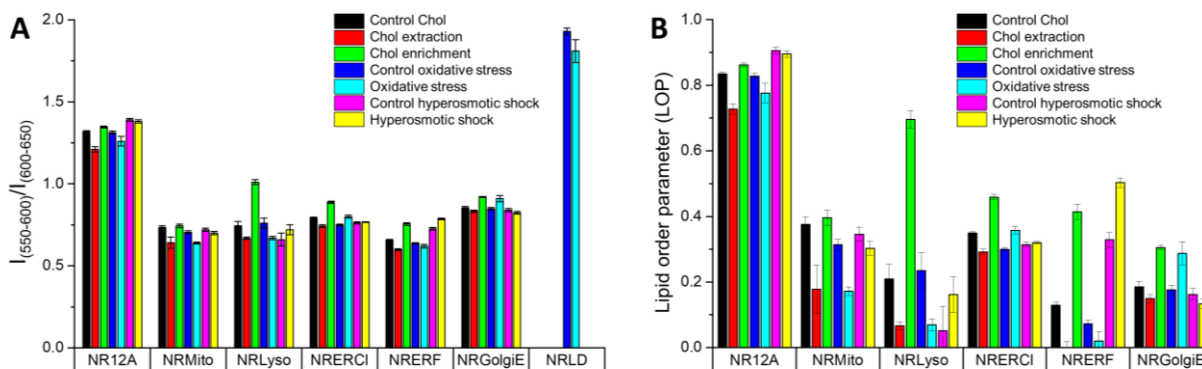


**Figure 6.** Quantitative analysis of fluorescence images of KB cells with solvatochromic probes for organelles after cholesterol extraction/enrichment, oxidative stress and hyperosmotic shock. (A) Weighted arithmetic mean values of green/red fluorescence intensities ratio ( $I_{550-600}/I_{600-650}$ ) and (B) lipid order parameter (LOP) values calculated from ratiometric images of organelle probes in KB cells and LUVs under various conditions.

Exposing cells to hydrogen peroxide ( $H_2O_2$ ) leads to induction of oxidative stress, which is expected to alter the polarity of organelle membranes due to lipid peroxidation.<sup>70</sup> First, colocalization imaging experiments with reference organelle markers confirmed that the  $H_2O_2$  treatment did not affect organelle-specificity of the new probes (Figure S7, see Table S2 for Pearson's correlation coefficients). Second, after treatment with  $H_2O_2$ , the pseudo-color in ratiometric images (Figures 7A and S8) changed in a different way within the studied organelles, reflecting green/red ratio (i.e. local polarity) changes (Figures 6). The most pronounced increase of polarity (decrease in the green/red ratio) was detected in case of LDs, lysosomes and mitochondria (Figures 6 and 7B). Relatively high response in case of LDs is in line with our previous results<sup>34</sup> indicating high sensitivity of these organelles to oxidative stress, supposedly due to large quantity of easily oxidizable unsaturated lipids. In case of lysosomes, the treatment also resulted in a significant polarity increase, possibly because the interior of lysosomes derives from extracellular medium and therefore these organelles are highly exposed to the action of  $H_2O_2$ . The observed increase in heterogeneity of lysosomal polarity values (broadening of distribution of the intensity ratio, Figure 7B) is in line with literature data.<sup>71</sup> The polarity increase in mitochondria correlates well with literature data concerning high sensitivity of mitochondria to the oxidative stress, which is directly linked to aging and apoptosis.<sup>72-73</sup> According to the LOP analysis, oxidative stress significantly decreased the lipid order in lysosomes and mitochondria, with LOP values reaching those after cholesterol extraction (Figure 6). Plasma membrane showed lower changes, supposedly due to large quantity of saturated lipids, less prone to oxidation. NRER<sub>Cl</sub> and especially NRGolgi<sub>E</sub> showed a decrease in polarity in comparison to intact cells. In case of NRGolgi<sub>E</sub>, this decrease is unexpected and could be related to increase in the fraction of unsaturated lipids and cholesterol because of oxidative stress. In addition, oxidative stress could alter the localization of the probe in the cells, even though they generally remain in the target organelles according to the colocalization data (see above). Overall, oxidative stress produced significant polarity/lipid order alternations in the membranes of the whole cell, with strongly varied response in different organelles.

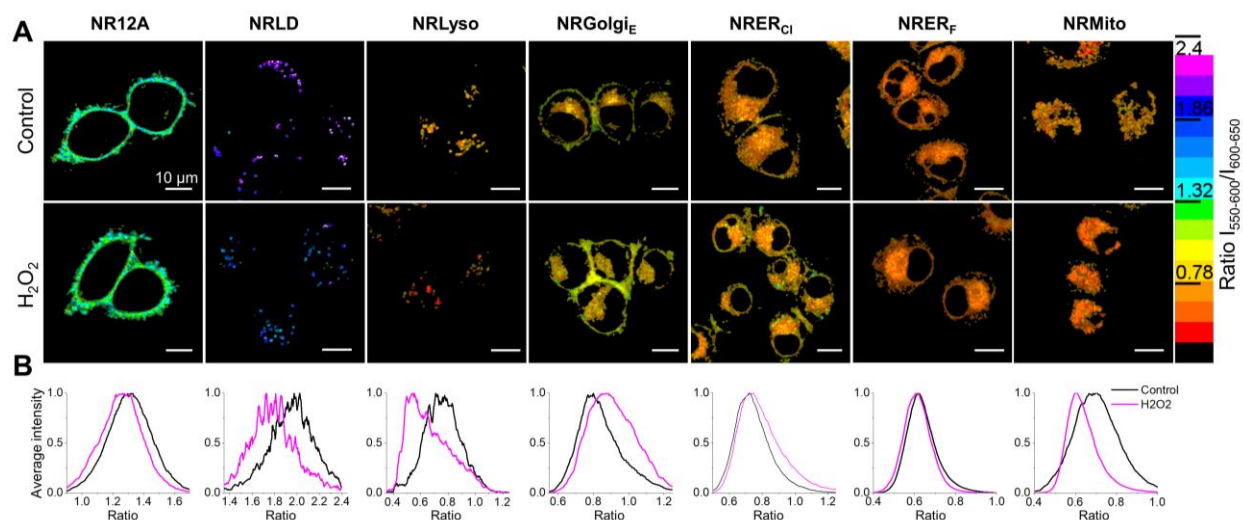


**Figure 7.** (A) Confocal ratiometric imaging of live KB cells under oxidative stress, using solvatochromic probes for organelles. The stress was produced by 2 mM hydrogen peroxide (1h at 37°C). Probe concentration 20 nM for NR12A; 50 nM for NRMito, NRLyso, NRLD, NRER<sub>Ci</sub>; 200 nM for NRER<sub>F</sub>; 5 μM (in form of BSA-conjugate) for NRGolgi<sub>E</sub>. (B) Distribution histogram of the green/red fluorescence intensity ratio ( $I_{550-600}/I_{600-650}$ ) for corresponding probes in KB cells.

Mechanobiology is a rapidly growing research field, which covers multiple aspects, including development,<sup>74</sup> collective cellular behavior,<sup>75</sup> tumor growth,<sup>76</sup> etc. As mechanical stress can directly affect lipid order of biomembranes, the fluorescent tools sensitive to membrane tension and viscosity have been recently proposed to monitor mechanical stress at the level of organelles.<sup>5,25,29</sup> A simple method to induce a mechanical stress in the cells is to change osmolality of the media, for example by hyperosmotic stress, accompanied by changes in lipid order and cell morphology.<sup>66,77</sup> Here, we studied the effect of hyperosmotic stress on organelles of live KB cells using our new probes for monitoring local polarity and lipid order. As in the case of oxidative stress, colocalization imaging experiments confirmed that hyperosmotic stress did not affect organelle-specificity of the new probes (Figure S9, see Table S2 for Pearson's correlation coefficients). Plasma membrane (stained with NR12A) upon induction of hyperosmotic stress exhibited a change in morphology, yielding a jagged pattern together with appearance of more polar (and less ordered) regions on the inner parts compared to the extremities (Figure 8 and S10). This could be attributed to the drop in lipid order in the most displaced parts of membrane driven by cell shrinkage. These observations are in line with the previous results,<sup>58</sup> as these innermost parts of plasma membrane seem to undergo more deformation, probably by stretching, compared to outmost ones. In the cell extremities the shrinkage is limited, probably due to a presence of rigid cytoskeleton filaments. Overall, the decrease in the LOP values (Figures 6) of PM reported by NR12A correlated with the decreased lipid order revealed by mechanosensitive flipper probe for PM.<sup>5,29</sup> A decrease in the LOP values (and increase in polarity) were also observed for mitochondria and Golgi apparatus, whereas lysosomes and ER showed the opposite effect (Figures 6 and 8). The observed lower LOP values in mitochondria membranes after hyperosmotic shock correlated well with the decrease in the lipid order and local viscosity reported by mitochondrial flipper<sup>5</sup> and molecular rotor<sup>25</sup> probes, respectively. It is also in line with a recent report on a solvatochromic mitochondria-specific probe.<sup>54</sup> The peculiar behavior of lysosomes (e.g. lower polarity and higher LOP) is

probably because they are expected to shrink, which induces higher lipid ordering at the inner leaflet of the vesicles, where NRLyso locates. It should be noted that the green/red intensity ratio of the probes in plasma membranes, lysosomes and ER (NRER<sub>F</sub>) (Figure 6A) varied within the control cells of different cell culture passages (cells in Figure 8 were ~8 passages older than those in Figure 7 and ~13 passages older than those in Figure 5). This interesting effect would require a dedicated study in order to verify whether polarity and lipid order of these biomembranes are also affected by cell aging. The two probes for ER yielded different response towards hyperosmotic stress: practically no response from NRER<sub>Cl</sub>, in contrast to a pronounced increase in the LOP values (and decrease in polarity) reported by NRER<sub>F</sub> (Figures 6 and 8). As NRER<sub>F</sub>, bearing polar PEG linker, is poorly inserted into the lipid membrane according to data in LUVs (Figure S2), cell shrinkage during hyperosmotic stress produces compaction of ER, which can force deeper insertion of the Nile Red moiety into the ER membranes. This result is in line with the previously reported increase in the local viscosity revealed by molecular rotors targeted to ER,<sup>25</sup> although in this case ER flipper probe showed some decrease in the lipid order.<sup>5</sup> Overall, mechanical stress in cells produced very different responses within organelles, probably because of different geometry and lipid composition of their membranes as well as different location of the probe within the bilayer leaflets and varied insertion of their fluorophore.

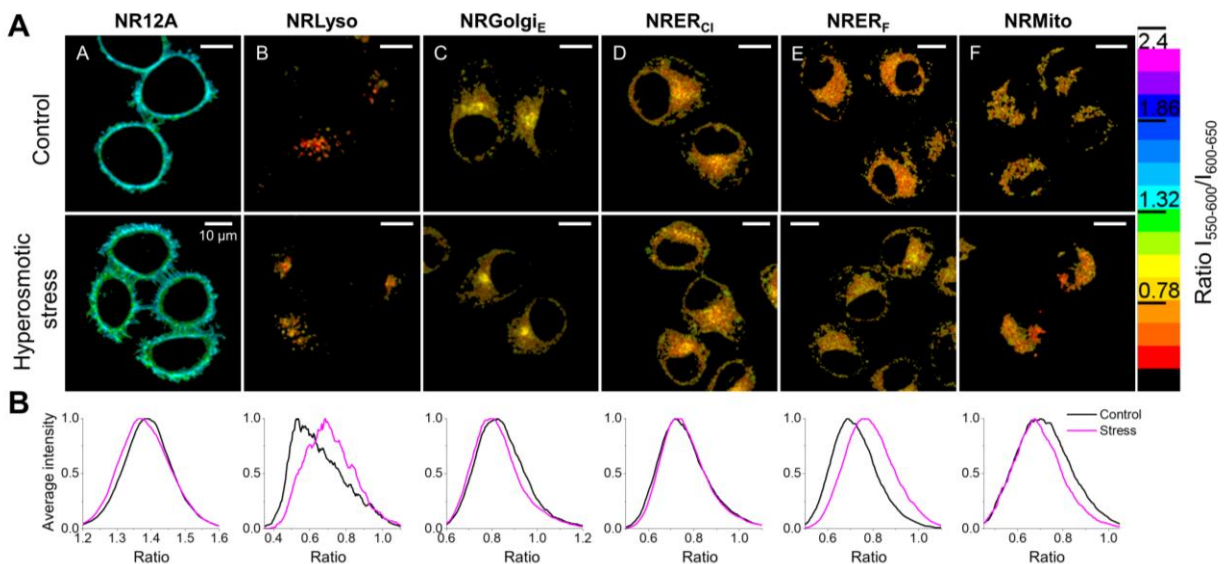


**Figure 8.** (A) Confocal ratiometric imaging of live KB cells under hyperosmotic shock, using solvatochromic probes for organelles. The shock was produced by replacing a half of the medium with 1 M sucrose solution. Probe concentration: 20 nM for NR12A; 50 nM for NRMito, NRLyso, NRLD, NRER<sub>Cl</sub>; 200 nM for NRER<sub>F</sub>; 5  $\mu$ M (in form of BSA-conjugate) for NRGolgi<sub>E</sub>. (B) Distribution histogram of the green/red fluorescence intensity ratio ( $I_{550-600}/I_{600-650}$ ) for corresponding probes in KB cells.

## CONCLUSIONS

In this work, we synthesized an array of organelle-targeted solvatochromic fluorescent probes based on Nile Red. Overall, the developed probes for ER, mitochondria, Golgi apparatus, lipid droplets, lysosomes and plasma membrane (from the earlier report<sup>58</sup>) are capable of selective organelle targeting with sensing the local polarity, revealing fine differences in their lipid order. As we used the same solvatochromic dye,

it became possible to directly compare local polarity for different organelles and thus establish the following trend: lipid droplets << plasma membrane << Golgi apparatus < lysosomes < ER < mitochondria < ER (with shallow probe NRER<sub>F</sub>). However, each probe, having different chemical design, reported slightly different local polarity even for the same model lipid membrane, as evidenced by spectroscopy and microscopy data in lipid vesicles. Therefore, to directly compare lipid order in different organelles, we developed a methodology to convert the observed local polarity into quantitative lipid order parameter, using calibration of each probe in model lipid bilayers of ordered and disordered phases. This approach allowed us to establish the first quantitative comparison of lipid order in biomembranes of different organelles, revealing the following trend, slightly different from that based on local polarity: plasma membrane >> mitochondria ~ ER > lysosomes > Golgi apparatus > ER (with shallow probe NRER<sub>F</sub>). All new probes showed ratiometric response to cholesterol depletion and enrichment, thus confirming that the probes sense lipid order in biomembranes of the studied organelles. Moreover, the effect of cholesterol enrichment was particularly strong in cholesterol-poor organelles, such as ER and lysosomes, in contrast to cholesterol-rich plasma membranes where the effect was very small.

The toolkit of solvatochromic probes revealed that organelles are differently sensitive to oxidative or hyperosmotic stress in terms of their local polarity and lipid order: lipid droplets, mitochondria and lysosomes being the most sensitive towards oxidative stress, where significant polarity increase was observed, probably due to modification of fatty acid chains with polar superoxide groups. On the other hand, lysosomes, ER (with shallow probe) and mitochondria showed the strongest response to hyperosmotic conditions. Moreover, hyperosmotic stress increased heterogeneity in the plasma membrane, possibly due to appearance of liquid disordered phase domains presumably at the places with the highest mechanical stress. Overall, the new solvatochromic probes enable deciphering fine changes in the local polarity and lipid order specifically in different organelles. However, a special care should be taken about the fluorophore insertion into bilayer controlled by polarity and bulkiness of the targeting group, because it may significantly alter the probe response. Even though the Nile Red moiety in these probes is lipophilic and preferentially localizes in lipid membranes, one cannot totally exclude an additional effect of membrane proteins, including those translocating between membrane and lumen of an organelle. The changes observed in organelles under mechanical stress by our solvatochromic probes correlate with those reported earlier by viscosity-sensitive molecular rotors and mechanosensitive flippers, although some differences have also been noticed. On the one hand, for all these three types of probes, the increase in lipid order produces profound changes in the bilayer, increasing viscosity and rigidity, while decreasing local polarity. On the other hand, different stress conditions (e.g. chemical and mechanical) could produce different effects on those three membrane parameters. A systematic work on comparing these three families of probes will be needed to understand better the fine differences in their response profiles. Overall, the present work highlights the importance of the use of the same fluorophore in the design of probes for studying and comparing properties of different target organelles. Moreover, it proposes an approach for quantitative comparison of local lipid order in organelles, based on calibration of probes in model vesicles with defined lipid order. Finally, this work proposes a toolkit of probes that can be directly used in cell biology, mechanobiology and biophysics for shedding light on the behavior of cellular organelles and their response to external stress.

## EXPERIMENTAL SECTION

**General methods and materials.** All the reagents were purchased from Sigma-Aldrich or Alfa Aesar or TCI and used as received. MilliQ-water (Millipore) was used in all experiments. NMR spectra were recorded at 20°C on BrukerAvance III 400 spectrometer. Mass spectra were obtained using an Agilent Q-TOF 6520 mass spectrometer. Absorption spectra were recorded on Cary 4000-HP spectrophotometer (Varian) and emission spectra were recorded on Fluoromax 4 (Jobin Yvon, Horiba) spectrofluorometer equipped with a thermostated cell compartment. Fluorescence quantum yields were measured using Nile Red (NR) in methanol ( $\lambda_{\text{ex}} = 520$  nm,  $\text{QY}_{\text{ref}} = 38\%$ )<sup>78</sup> as a reference. Compounds **1** and **NR12A** were synthesized according to the previously published procedure.<sup>58</sup>

**(3-(4-(Ethyl(5-oxo-5H-benzo[a]phenoxazin-9-yl)amino)butanamido)propyl)triphenylphosphonium (NRMito).** 30 mg of compound **1** were dissolved in 1 mL of dry DMF together with 31.9 mg (1.05 eq.) of HATU, 5.4 mg (0.5 eq.) of HOBt and 61.9 mg (6 eq., 84  $\mu\text{L}$ ) of DIPEA under Ar atmosphere. After 5 minutes, a solution of 40.3 mg (1.05 eq.) of 3-aminopropyltriphenylphosphonium bromide in 1 mL of dry DMF was added and the mixture was stirred for 24h (control by TLC) under Ar atmosphere. After the reaction the solvent was evaporated *in vacuo* and the product was purified by preparative TLC ( $\text{SiO}_2$ ,  $\text{DCM}:\text{MeOH}$  92:8). After the TLC the traces of DMF were removed by washing the crystalline product on a filter twice with diethyl ether and drying. Yield: 26 mg (43.0%) as a dark red solid.  $^1\text{H}$  NMR (400 MHz,  $\text{CDCl}_3$ )  $\delta$  ppm 8.66 (d,  $J=7.5$  Hz, 1 H) 8.31 (dd,  $J=7.8$ , 1.0 Hz, 1 H) 7.58 - 7.82 (m, 18 H) 6.86 (br t,  $J=6.0$  Hz, 1 H) 6.76 (dd,  $J=9.2$ , 2.6 Hz, 1 H) 6.57 (d,  $J=2.5$  Hz, 1 H) 6.36 (s, 1 H) 3.37 - 3.54 (m, 6 H) 3.16 - 3.27 (m, 2 H) 2.38 (br t,  $J=7.0$  Hz, 2 H) 1.86 - 2.02 (m, 4 H) 1.25 (t,  $J=7.0$  Hz, 3 H).  $^{13}\text{C}$  NMR (101 MHz,  $\text{CDCl}_3$ )  $\delta$  ppm 183.66 ( $\text{C}_{\text{ar}}$ ) 173.59 ( $\text{C}_{\text{amide}}$ ) 152.16 ( $\text{C}_{\text{ar}}$ ) 151.12 ( $\text{C}_{\text{ar}}$ ) 146.68 ( $\text{C}_{\text{ar}}$ ) 139.53 ( $\text{C}_{\text{ar}}$ ) 135.37 ( $\text{C}_{\text{ar}}$ ) 133.24 (d,  $J=10.0$  Hz,  $\text{C}_{\text{ar}}$ ) 132.07 ( $\text{C}_{\text{ar}}$ ) 131.65 ( $\text{C}_{\text{ar}}$ ) 131.22 (d,  $J=11.4$  Hz,  $\text{C}_{\text{ar}}$ ) 130.64 (d,  $J=12.65$  Hz,  $\text{C}_{\text{ar}}$ ) 129.79 ( $\text{C}_{\text{ar}}$ ) 125.57 ( $\text{C}_{\text{ar}}$ ) 125.01 ( $\text{C}_{\text{ar}}$ ) 123.75 ( $\text{C}_{\text{ar}}$ ) 118.15 ( $\text{C}_{\text{ar}}$ ) 117.29 ( $\text{C}_{\text{ar}}$ ) 110.15 ( $\text{C}_{\text{ar}}$ ) 105.48 ( $\text{C}_{\text{ar}}$ ) 96.42 ( $\text{C}_{\text{ar}}$ ) 50.22 ( $\text{C}_{\text{al}}$ ) 45.56 ( $\text{C}_{\text{al}}$ ) 39.14 (d,  $J=17.8$  Hz,  $\text{C}_{\text{al}}$ ) 32.82 ( $\text{C}_{\text{al}}$ ) 23.25 ( $\text{C}_{\text{al}}$ ) 22.49 (d,  $J=3.5$  Hz,  $\text{C}_{\text{al}}$ ) 20.17 (d,  $J=53.5$  Hz,  $\text{C}_{\text{al}}$ ) 12.36 (s,  $\text{C}_{\text{al}}$ ). HRMS (ESI),  $m/z$ :  $[\text{M}]^+$  calcd for  $\text{C}_{43}\text{H}_{41}\text{N}_3\text{O}_3\text{P}$ , 678.2880; found, 678.2889.

**4-(Ethyl(5-oxo-5H-benzo[a]phenoxazin-9-yl)amino)-N-(3-morpholinopropyl)butanamide (NRLyso).** 30 mg of compound **1** were dissolved in 2 mL of dry DMF together with 31.9 mg (1.05 eq.) of HATU, 5.4 mg (0.5 eq.) of HOBt and 41.2 mg (4 eq., 56  $\mu\text{L}$ ) of DIPEA under Ar atmosphere. After 5 minutes, 12.1 mg (1.05 eq, 12.2  $\mu\text{L}$ ) of 3-morpholinopropylamine were added and the mixture was stirred for 24h (control by TLC) under Ar atmosphere. After the reaction the solvent was evaporated *in vacuo* and the crude product was purified by preparative TLC (two consecutive purifications,  $\text{SiO}_2$ ;  $\text{DCM}:\text{MeOH}$  90:10). Yield: 6 mg (15.0%) as a dark red solid.  $^1\text{H}$  NMR (400 MHz,  $\text{CDCl}_3$ )  $\delta$  ppm 8.63 (dd,  $J=8.2$ , 1.1 Hz, 1 H) 8.29 (dd,  $J=7.8$ , 1.0 Hz, 1 H) 7.72 (td,  $J=8.0$ , 1.8 Hz, 1 H) 7.65 (td,  $J=7.8$ , 1.0 Hz, 1 H) 7.58 (d,  $J=9.3$  Hz, 1 H) 7.07 (br t,  $J=4.5$  Hz, 1 H) 6.69 (dd,  $J=9.3$ , 2.8 Hz, 1 H) 6.49 (d,  $J=2.8$  Hz, 1 H) 6.36 (s, 1 H) 3.68 (t,  $J=4.6$  Hz, 4 H) 3.42 - 3.52 (m, 4 H) 3.39 (q,  $J=6.0$  Hz, 2 H) 2.38 - 2.51 (m, 6 H) 2.26 (t,  $J=7.0$  Hz, 2 H) 2.00 (quin,  $J=7.3$  Hz, 2 H) 1.70 (quin,  $J=6.3$  Hz, 2 H) 1.25 (t,  $J=7.2$  Hz, 3 H).  $^{13}\text{C}$  NMR (101 MHz,  $\text{DMSO}-d_6$ )  $\delta$  ppm 183.76 ( $\text{C}_{\text{ar}}$ ) 171.60 ( $\text{C}_{\text{amide}}$ ) 152.10 ( $\text{C}_{\text{ar}}$ ) 150.97 ( $\text{C}_{\text{ar}}$ ) 146.65 ( $\text{C}_{\text{ar}}$ ) 140.11 ( $\text{C}_{\text{ar}}$ ) 132.04 ( $\text{C}_{\text{ar}}$ ) 131.72 ( $\text{C}_{\text{ar}}$ ) 131.35 ( $\text{C}_{\text{ar}}$ ) 131.12 ( $\text{C}_{\text{ar}}$ ) 129.97 ( $\text{C}_{\text{ar}}$ ) 125.65 ( $\text{C}_{\text{ar}}$ ) 125.03 ( $\text{C}_{\text{ar}}$ ) 123.83 ( $\text{C}_{\text{ar}}$ ) 109.91 ( $\text{C}_{\text{ar}}$ ) 105.72 ( $\text{C}_{\text{ar}}$ ) 96.54 ( $\text{C}_{\text{ar}}$ ) 67.05 ( $\text{C}_{\text{al}}$ ) 57.81 ( $\text{C}_{\text{al}}$ ) 53.68 ( $\text{C}_{\text{al}}$ ) 49.95 ( $\text{C}_{\text{al}}$ ) 45.44 ( $\text{C}_{\text{al}}$ ) 39.45 ( $\text{C}_{\text{al}}$ ) 33.18 ( $\text{C}_{\text{al}}$ ) 24.93 ( $\text{C}_{\text{al}}$ ) 23.20 ( $\text{C}_{\text{al}}$ ) 12.35 ( $\text{C}_{\text{al}}$ ). HRMS (ESI),  $m/z$ :  $[\text{M}+\text{H}]^+$  calcd for  $\text{C}_{29}\text{H}_{35}\text{N}_4\text{O}_4$ , 503.2659; found, 503.2679.

**Tert-butyl (1-oxo-1-(perfluorophenyl)-5,8,11,14,17,20,23,26,29,32,35-undeca-oxa-2-azaheptatriacontan-37-yl)carbamate (2a).** 260 mg of BocHN-PEG<sub>11</sub>-NH<sub>2</sub> were dissolved in 5 mL of dry DCM together with 730 mg (5.5 eq.) of Cs<sub>2</sub>CO<sub>3</sub> and the mixture was cooled to 0 °C in an ice bath. Then, 415 mg (4.5 eq., 260 µL) of pentafluorobenzoyl chloride were added and the mixture was stirred for 1h at 0 °C and then for 1h at r.t. under Ar atmosphere. After the reaction the solvent was evaporated *in vacuo*, then 98.7 µL of TFA together with 10 mL of DCM were added to neutralize Cs<sub>2</sub>CO<sub>3</sub>. After this the solid residue was filtered off, and the solvent was evaporated *in vacuo*. The crude product was purified by column chromatography (SiO<sub>2</sub>; DCM:MeOH 95:5, alkaline KMnO<sub>4</sub> staining for TLC analysis of the column fractions). Yield: 259 mg (76.6 %) as a colourless oil. <sup>1</sup>H NMR (400 MHz, CDCl<sub>3</sub>) δ ppm 7.09 (br s, 1 H) 5.04 (br s, 1 H) 3.55 - 3.69 (m, 44 H) 3.53 (br t, *J*=5.1 Hz, 1 H) 3.30 (br q, *J*=5.0 Hz, 2 H) 2.43 (br s, 1 H) 1.43 (s, 9 H). <sup>13</sup>C NMR (101 MHz, DMSO-*d*<sub>6</sub>) δ ppm 157.44 (C<sub>carbox</sub>) 156.00 (C<sub>carbox</sub>) 145.29 (C<sub>ar</sub>) 142.83 (C<sub>ar</sub>) 138.81 (C<sub>ar</sub>) 136.27 (C<sub>ar</sub>) 112.04 (d, *J*=3.7 Hz, C<sub>ar</sub>) 78.71 - 79.49 (m, C<sub>al</sub>) 70.48 - 70.62 (m, C<sub>al</sub>) 70.47 (C<sub>al</sub>) 70.45 (C<sub>al</sub>) 70.43 (C<sub>al</sub>) 70.37 (C<sub>al</sub>) 70.26 (C<sub>al</sub>) 70.21 (C<sub>al</sub>) 69.35 (C<sub>al</sub>) 40.38 (C<sub>al</sub>) 40.15 (C<sub>al</sub>) 28.41 (C<sub>al</sub>). HRMS (ESI), *m/z*: [M+Na]<sup>+</sup> calcd for C<sub>36</sub>H<sub>59</sub>F<sub>5</sub>N<sub>2</sub>O<sub>14</sub>Na, 861.3786; found, 861.3807.

**N-(35-Amino-3,6,9,12,15,18,21,24,27,30,33-undeca-oxapentatriacontyl)-2,3,4,5,6-pentafluorobenzamide (2b).** 240 mg of **1a** were dissolved in 2 mL of dry DCM, after that 2 mL of TFA were added and the mixture was stirred for 2h at r.t. After the reaction the solvent was evaporated *in vacuo*. In order to eliminate traces of TFA, 1 mL of methanol was added, followed by evaporation *in vacuo* (3 times). Yield: 238 mg (97.2%) as a colourless oil. <sup>1</sup>H NMR (400 MHz, CDCl<sub>3</sub>) δ ppm 7.43 (br s, 1 H) 7.02 (br s, 1 H) 3.78 (t, *J*=5.3 Hz, 2 H) 3.58 - 3.71 (m, 44 H) 3.15 (sxt, *J*=5.4 Hz, 2 H). <sup>13</sup>C NMR (101 MHz, DMSO-*d*<sub>6</sub>) δ ppm 176.96 (C<sub>amide</sub>) 159.68 (q, *J*=39.40 Hz, C<sub>ar</sub>) 158.36 (C<sub>ar</sub>) 115.33 (q, *J*=287.69 Hz, C<sub>ar</sub>) 70.26 (C<sub>al</sub>) 70.23 (C<sub>al</sub>) 70.15 (C<sub>al</sub>) 70.12 (C<sub>al</sub>) 70.09 (C<sub>al</sub>) 70.04 (C<sub>al</sub>) 70.01 (C<sub>al</sub>) 69.89 (C<sub>al</sub>) 69.84 (C<sub>al</sub>) 69.79 (C<sub>al</sub>) 69.78 (C<sub>al</sub>) 69.74 (C<sub>al</sub>) 69.70 (C<sub>al</sub>) 69.63 (C<sub>al</sub>) 69.55 (C<sub>al</sub>) 69.41 (C<sub>al</sub>) 69.16 (C<sub>al</sub>) 66.64 (C<sub>al</sub>) 40.13 (C<sub>al</sub>) 39.78 (C<sub>al</sub>) 21.97 (C<sub>al</sub>). HRMS (ESI), *m/z*: [M+H]<sup>+</sup> calcd for C<sub>31</sub>H<sub>52</sub>F<sub>5</sub>N<sub>2</sub>O<sub>12</sub>, 739.3441; found, 739.3471.

**2,3,4,5,6-Pentafluoro-N-(37-oxo-41-(5-oxo-5H-benzo[a]phenoxazin-9-yl)-6,9,12,15,18,21,24,27,30,33-undeca-oxa-36,41-diazatritetracontyl)benzamide (NRER<sub>F</sub>).** 30 mg of compound **1** were dissolved in 1 mL of dry DMF together with 31.9 mg (1.05 eq.) of HATU, 5.4 mg (0.5 eq.) of HOBT and 61.9 mg (6 eq., 84 µL) of DIPEA under Ar atmosphere. After 5 minutes, a solution of 71.4 mg (1.05 eq.) of **2b** in 1 mL of dry DMF was added and the mixture was stirred for 24h (control by TLC) under Ar atmosphere. After the reaction the solvent was evaporated *in vacuo*. The crude product was purified by preparative TLC (SiO<sub>2</sub>, DCM:MeOH 95:5). Yield: 53 mg (60.6 %) as a dark red oil. <sup>1</sup>H NMR (400 MHz, CDCl<sub>3</sub>) δ ppm 8.62 (d, *J*=7.5 Hz, 1 H) 8.25 (d, *J*=7.5 Hz, 1 H) 7.70 (td, *J*=7.53, 1.2 Hz, 1 H) 7.62 (td, *J*=7.53, 1.2 Hz, 1 H) 7.57 (d, *J*=9.3 Hz, 1 H) 7.32 - 7.40 (m, 1 H) 6.70 (dd, *J*=9.0, 2.5 Hz, 1 H) 6.56 (br t, *J*=4.5 Hz, 1 H) 6.49 (d, *J*=2.5 Hz, 1 H) 6.35 (s, 1 H) 3.55-3.69 (m, 44 H) 3.39 - 3.50 (m, 8 H) 2.30 (br t, *J*=7.0 Hz, 2 H) 1.98 (quin, *J*=7.3 Hz, 2 H) 1.23 (t, *J*=7.0 Hz, 3 H). <sup>13</sup>C NMR (101 MHz, DMSO-*d*<sub>6</sub>) δ ppm 183.73 (C<sub>ar</sub>) 172.34 (C<sub>amide</sub>) 157.63 (C<sub>amide</sub>) 152.18 (C<sub>ar</sub>) 151.09 (C<sub>ar</sub>) 146.68 (C<sub>ar</sub>) 145.29 (C<sub>ar</sub>) 142.74 (C<sub>ar</sub>) 139.71 (C<sub>ar</sub>) 138.77 (C<sub>ar</sub>) 136.28 (C<sub>ar</sub>) 132.05 (C<sub>ar</sub>) 131.62 (C<sub>ar</sub>) 131.33 (C<sub>ar</sub>) 131.17 (C<sub>ar</sub>) 129.86 (C<sub>ar</sub>) 125.57 (C<sub>ar</sub>) 125.09 (C<sub>ar</sub>) 123.79 (C<sub>ar</sub>) 112.09 (d, *J*=3.7 Hz, C<sub>ar</sub>) 110.11 (C<sub>ar</sub>) 105.52 (C<sub>ar</sub>) 96.46 (C<sub>ar</sub>) 70.41 (C<sub>al</sub>) 70.35 (C<sub>al</sub>) 70.28 (C<sub>al</sub>) 70.27 (C<sub>al</sub>) 70.21 (C<sub>al</sub>) 70.18 (C<sub>al</sub>) 70.07 (C<sub>al</sub>) 69.89 (C<sub>al</sub>) 69.42 (C<sub>al</sub>) 50.64 (C<sub>al</sub>) 50.09 (C<sub>al</sub>) 45.50 (C<sub>al</sub>) 40.11 (C<sub>al</sub>) 39.26 (C<sub>al</sub>) 32.86 (C<sub>al</sub>) 23.13 (C<sub>al</sub>) 12.35 (C<sub>al</sub>). HRMS (ESI), *m/z*: [M+Na]<sup>+</sup> calcd for C<sub>53</sub>H<sub>69</sub>F<sub>5</sub>N<sub>4</sub>O<sub>15</sub>Na, 1119.4580; found, 1119.4619.



**N-(3-Chloropropyl)-4-(ethyl(5-oxo-5H-benzo[a]phenoxazin-9-yl)amino)butanamide (NRER<sub>Cl</sub>)**. 30 mg of compound **1** were dissolved in 1 mL of dry DMF together with 31.9 mg (1.05 eq.) of HATU, 5.4 mg (0.5 eq.) of HOBt and 61.9 mg (6 eq., 84  $\mu$ L) of DIPEA under Ar atmosphere. After 5 minutes, a solution of 10.9 mg (1.05 eq.) of 3-chloropropylamine in 1 mL of dry DMF was added and the mixture was stirred for 24h (control by TLC) under Ar atmosphere. After the reaction the solvent was evaporated *in vacuo*, then the solid residue was dissolved in EtOAc and washed with water (x3), dried over Na<sub>2</sub>SO<sub>4</sub> and the solvent was evaporated *in vacuo*. The crude product was purified by preparative TLC (SiO<sub>2</sub>, DCM:MeOH 98:2). Yield: 14 mg (38.9 %) as a dark red solid. <sup>1</sup>H NMR (400 MHz, CDCl<sub>3</sub>)  $\delta$  ppm 8.61 (dd, *J*=8.0, 0.8 Hz, 1 H) 8.22 (dd, *J*=7.9, 0.9 Hz, 1 H) 7.70 (td, *J*=7.6, 1.3 Hz, 1 H) 7.62 (td, *J*=7.6, 1.0 Hz, 1 H) 7.54 (d, *J*=9.0 Hz, 1 H) 6.68 (dd, *J*=9.0, 2.8 Hz, 1 H) 6.48 (d, *J*=2.8 Hz, 1 H) 6.32 (s, 1 H) 6.24 (br t, *J*=5.8 Hz, 1 H) 3.59 (t, *J*=6.4 Hz, 2 H) 3.37 - 3.50 (m, 6 H) 2.31 (t, *J*=7.2 Hz, 2 H) 1.94 - 2.06 (m, 4 H) 1.22 (t, *J*=7.2 Hz, 3 H). <sup>13</sup>C NMR (101 MHz, DMSO-*d*<sub>6</sub>)  $\delta$  ppm 183.77 (C<sub>ar</sub>) 172.50 (C<sub>amide</sub>) 152.38 (C<sub>ar</sub>) 151.24 (C<sub>ar</sub>) 146.71 (C<sub>ar</sub>) 139.33 (C<sub>ar</sub>) 132.09 (C<sub>ar</sub>) 131.51 (C<sub>ar</sub>) 131.42 (C<sub>ar</sub>) 131.25 (C<sub>ar</sub>) 129.83 (C<sub>ar</sub>) 125.45 (C<sub>ar</sub>) 125.32 (C<sub>ar</sub>) 123.89 (C<sub>ar</sub>) 110.33 (C<sub>ar</sub>) 105.19 (C<sub>ar</sub>) 96.45 (C<sub>ar</sub>) 55.60 (C<sub>al</sub>) 50.07 (C<sub>al</sub>) 45.52 (C<sub>al</sub>) 37.17 (C<sub>al</sub>) 33.09 (C<sub>al</sub>) 32.15 (C<sub>al</sub>) 23.25 (C<sub>al</sub>) 12.36 (C<sub>al</sub>). HRMS (ESI), *m/z*: [M-H-Cl+Na]<sup>+</sup> calcd for C<sub>25</sub>H<sub>25</sub>N<sub>3</sub>O<sub>3</sub>Na, 438.1796; found, 438.1802.

**Tert-butyl (2-dodecanamidoethyl)carbamate (3a)**. 0.5 g of myristic acid were dissolved in 5 mL of dry DMF together with 874 mg (1.05 eq.) of HATU, 148 mg (0.5 eq.) of HOBt and 850 mg (3 eq., 1.15 mL) of DIPEA under Ar atmosphere. After 5 minutes, a solution of 368 mg (1.05 eq.) of N-Boc-ethylenediamine in 5 mL of dry DMF was added and the mixture was stirred for 24h (control by TLC). After the reaction the solvent was evaporated *in vacuo* and the product was purified by column chromatography (SiO<sub>2</sub>, DCM:MeOH 95:5). Yield: 670 mg (80.6 %) as a pale yellowish solid. <sup>1</sup>H NMR (400 MHz, CDCl<sub>3</sub>)  $\delta$  ppm 6.10 (br s, 1 H) 4.88 (br s, 1 H) 3.32 - 3.39 (m, 2 H) 3.22 - 3.31 (m, 2 H) 2.16 (t, *J*=8.0 Hz, 2 H) 1.61 (m, 4 H) 1.44 (s, 9 H) 1.20 - 1.34 (m, 18 H) 0.88 (t, *J*=6.8 Hz, 3 H).

**N-(2-Aminoethyl)dodecanamide (3b)**. 240 mg of **3a** were dissolved in 2 mL of dry DCM, after that 2 mL of TFA were added and the mixture was stirred for 2h at r.t. After the reaction the solvent was evaporated *in vacuo*. In order to eliminate traces of TFA, 1 mL of methanol was added, followed by evaporation *in vacuo* (3 times). Yield: 241.9 mg (97.0 %) (in a form of TFA salt) as a pale yellowish solid. <sup>1</sup>H NMR (400 MHz, CDCl<sub>3</sub>)  $\delta$  ppm 7.37 (br s, 1 H) 3.45 - 3.58 (m, 2 H) 3.05 - 3.21 (m, 2 H) 1.48 - 1.61 (m, 2 H) 1.17 - 1.33 (m, 20 H) 0.87 (t, *J*=7.0 Hz, 3 H).

**N-(2-(4-(Ethyl(5-oxo-5H-benzo[a]phenoxazin-9-yl)amino)butanamido)ethyl)tetradecanamide (NRGolg<sub>E</sub>)**. 30 mg of compound **1** were dissolved in 1 mL of dry DMF together with 31.9 mg (1.05 eq.) of HATU, 5.4 mg (0.5 eq.) of HOBt and 41.23 mg (4 eq., 55.6  $\mu$ L) of DIPEA under Ar atmosphere. After 5 minutes, a solution of 22.7 mg (1.05 eq.) of **3b** and 28  $\mu$ L of DIPEA in 1 mL of dry DCM was added and the mixture was stirred for 24h (control by TLC) under Ar atmosphere. After the reaction the solvent was evaporated *in vacuo* and the crude product was separated by preparative TLC. Yield: 22 mg (43.9 %) as a dark red solid. <sup>1</sup>H NMR (400 MHz, CDCl<sub>3</sub>)  $\delta$  ppm 8.63 (d, *J*=7.8 Hz, 1 H) 8.25 (d, *J*=7.8 Hz, 1 H) 7.71 (td, *J*=7.5, 1.0 Hz, 1 H) 7.63 (br td, *J*=7.5, 1.0 Hz, 1 H) 7.56 (d, *J*=9.0 Hz, 1 H) 6.82 (br s, 1 H) 6.69 (dd, *J*=9.0, 2.5 Hz, 1 H) 6.46 - 6.53 (m, 2 H) 6.35 (s, 1 H) 3.35 - 3.52 (m, 8 H) 2.31 (t, *J*=7.3 Hz, 2 H) 2.18 (t, *J*=7.7 Hz, 2 H) 1.93 - 2.03 (m, 2 H) 1.53 - 1.63 (m, 2 H) 1.16 - 1.32 (m, 23 H) 0.87 (t, *J*=6.9 Hz, 3 H). The <sup>13</sup>C

NMR spectra could not be obtained due to limited solubility of the probe. HRMS (ESI),  $m/z$ :  $[M+Na]^+$  calcd for  $C_{38}H_{52}N_4O_4Na$ , 651.3889; found, 651.3902.

**N,N-Dicyclohexyl-4-(ethyl(5-oxo-5H-benzo[a]phenoxazin-9-yl)amino)butanamide (NRLD).** 30 mg of compound **1** were dissolved in 1 mL of dry DMF together with 31.9 mg (1.05 eq.) of HATU, 5.4 mg (0.5 eq.) of HOBt and 51 mg (5 eq., 70  $\mu$ L) of DIPEA under Ar atmosphere. After 5 minutes, a solution of 15.2 mg (1.05 eq., 16.7  $\mu$ L) of dicyclohexylamine in 1 mL of dry DMF was added and the mixture was stirred for 24h (control by TLC) under Ar atmosphere. After the reaction the solvent was evaporated *in vacuo*, the solid residue was dissolved in DCM, washed with water and brine, dried over  $Na_2SO_4$ , then the solvent was evaporated *in vacuo*. The crude product was purified by preparative TLC (two consecutive purifications,  $SiO_2$ ; DCM:MeOH 99:1 and  $SiO_2$ ; DCM:MeOH 98:2, respectfully). Yield: 30 mg (67.5 %) as a dark red solid.  $^1H$  NMR (400 MHz,  $CDCl_3$ )  $\delta$  ppm 8.63 (dd,  $J=8.0, 0.8$  Hz, 1 H) 8.29 (dd,  $J=7.8, 1.0$  Hz, 1 H) 7.71 (td,  $J=7.5, 1.5$  Hz, 1 H) 7.63 (td,  $J=7.5, 1.5$  Hz, 1 H) 7.58 (d,  $J=9.0$  Hz, 1 H) 6.70 (dd,  $J=9.3, 2.8$  Hz, 1 H) 6.50 (d,  $J=2.8$  Hz, 1 H) 6.36 (s, 1 H) 3.43 - 3.51 (m, 5 H) 2.40 - 2.60 (m, 2 H) 2.36 (t,  $J=6.5$  Hz, 2 H) 1.97 (quin,  $J=7.0$  Hz, 2 H) 1.76 - 1.87 (m, 4 H) 1.59 - 1.70 (m, 4 H) 1.46 - 1.57 (m, 4 H) 1.03 - 1.33 (m, 10 H).  $^{13}C$  NMR (101 MHz,  $DMSO-d_6$ )  $\delta$  ppm 183.72 ( $C_{ar}$ ) 170.60 ( $C_{amide}$ ) 152.14 ( $C_{ar}$ ) 151.17 ( $C_{ar}$ ) 146.69 ( $C_{ar}$ ) 139.91 ( $C_{ar}$ ) 132.07 ( $C_{ar}$ ) 131.74 ( $C_{ar}$ ) 131.27 ( $C_{ar}$ ) 131.08 ( $C_{ar}$ ) 129.87 ( $C_{ar}$ ) 125.66 ( $C_{ar}$ ) 124.99 ( $C_{ar}$ ) 123.76 ( $C_{ar}$ ) 109.97 ( $C_{ar}$ ) 105.67 ( $C_{ar}$ ) 96.52 ( $C_{ar}$ ) 50.10 ( $C_{al}$ ) 45.40 ( $C_{al}$ ) 30.22 ( $C_{al}$ ) 26.66 ( $C_{al}$ ) 26.09 ( $C_{al}$ ) 25.42 ( $C_{al}$ ) 25.23 ( $C_{al}$ ) 22.99 ( $C_{al}$ ) 12.36 ( $C_{al}$ ). HRMS (ESI),  $m/z$ :  $[M+Na]^+$  calcd for  $C_{22}H_{20}N_2O_4Na$ , 562.3048; found, 562.3062.

**Preparation of liposomes.** All types of large unilamellar vesicles (LUVs) used were prepared by the following procedure. A stock solution of corresponding lipid(s) in chloroform was placed into a round-neck flask, after which the solvent was evaporated *in vacuo* and phosphate buffer (20 mM, pH 7.4) was added. After all the solid was dissolved a suspension of multilamellar vesicles was extruded by using a Lipex Biomembranes extruder (Vancouver, Canada). The size of the filters was first 0.2  $\mu$ m (7 passages) and thereafter 0.1  $\mu$ m (10 passages). This generates monodisperse LUVs with a mean diameter of 0.12  $\mu$ m as measured with a Malvern Zetamaster 300 (Malvern, U.K.). Phospholipid:Cholesterol molar ratio in case of DOPC/Chol and Sphing/Chol was 1:0.9.

**Cell Lines, Culture Conditions, and Treatment.** HeLa cells (ATCC CCL-2) cells were grown in Dulbecco's Modified Eagle Medium (DMEM, Gibco Invitrogen), supplemented with 10% fetal bovine serum (FBS, Lonza), 1% l-Glutamine (Sigma Aldrich) and 1% antibiotic solution (penicillin-streptomycin, Gibco-Invitrogen) at 37 °C in a humidified 5%  $CO_2$  atmosphere. KB (ATCC CCL-17) cells were grown in Dulbecco's Modified Eagle Medium (DMEM, Gibco Invitrogen), supplemented with 10% fetal bovine serum (FBS, Lonza), 1% l-Glutamine (Sigma Aldrich), 1% non-essential amino acid solution (Gibco-Invitrogen) and 1% MEM vitamin solution (Gibco-Invitrogen) at 37 °C in a humidified 5%  $CO_2$  atmosphere. Cells were seeded onto a chambered coverglass (IBiDi) at a density of  $5 \times 10^4$  cells/well 24 h before the microscopy measurement. For microscopy imaging, the attached cells in ABIDI dishes were washed once with warm Hanks' balanced salt solution (HBSS, Gibco-Invitrogen), after that 1 mL of corresponding dye solution in warm HBSS was added and the cells were incubated for: 10 min. at r.t. for NR12A, NRLipD or Nile Red; 20 min at 37 °C for NRER<sub>F</sub> and NRER<sub>Cl</sub>; 45 min at 37 °C for NRLyso and NRMito. For NRGolgi<sub>E</sub> probe the attached cells in ABIDI dishes were washed twice with cold Hanks' balanced salt solution (HBSS, Gibco-Invitrogen), after that 1 mL of cold solution of dye conjugate with

BSA (1:1 molar ratio) or with  $\beta$ -cyclodextrine (1:6 molar ratio) was added and the cells were incubated for 30 min at 4 °C followed by washing with warm HBSS and further incubation for 30 min at 37 °C.

For colocalization experiments, commercial organelle-targeting probes were added together with solvatochromic probes in the following concentrations: 50 nM of WGA Alexa 488 conjugate (Invitrogen) for NR12A; 50 nM of MitoTracker Green FM (Invitrogen) for NRMito; 50 nM of LysoTracker Green DND-26 (Invitrogen) for NRLyso; 200 nM (for NRER<sub>F</sub>) or 500 nM (for NRER<sub>Cl</sub>) of ERTracker Green (Invitrogen); 500 nM of BODIPY 493/503 (Invitrogen) for NRLipD; 2.5  $\mu$ M (in form of 1:1 molar ratio conjugate with BSA) or 150 nM (in 1 mM solution of  $\beta$ -cyclodextrine) of BODIPY FL C<sub>5</sub>-Ceramide (Invitrogen) for NRGolgi<sub>E</sub>.

**Fluorescence microscopy.** Cellular imaging was performed using Nikon Ti-E inverted microscope, equipped with CFI Plan Apo  $\times$ 60 oil (NA = 1.4) objective, X-Light spinning disk module (CREST Optics) and a Hamamatsu Orca Flash 4 sCMOS camera with a bandpass filter 531/40 nm (Semrock) or 600/50 nm (Semrock). The excitation in confocal mode was provided by 488 nm or 532 nm diode laser (OXXIUS). The exposure time in confocal mode was set to 500 ms per image frame. All the images were recorded using NIS Elements and then processed using Fiji software. Pearson's correlation coefficients for colocalization were calculated using Coloc2 Fiji plugin.

Ratiometric confocal imaging of KB cells and LUVs was performed on a Leica TSC SPE confocal microscope with HXC PL APO 63x/1.40 OIL CS objective. The excitation light was provided by a 488 nm laser while the fluorescence was detected at two spectral ranges: 550–600 nm ( $I_{550-600}$ ) and 600–650 nm ( $I_{600-650}$ ) in sequential mode by rapid switching to minimize drift, a sum of 5 images is shown (20 images in case of hyperosmotic stress experiments with NR12A). All the parameters at each channel were left constant, illumination power was adjusted to achieve good signal for each probe. The laser power settings were: 8% of max. intensity for NRLipD; 9% of max. intensity for NRLyso; 12% of max. intensity for NRER<sub>Cl</sub> and NRMito; 30% of max. intensity for NR12A for oxidative stress experiments and 60% for hyperosmotic stress experiments; 45% of max. intensity for NRER<sub>F</sub>; 70% of max. intensity for NRGolgi<sub>E</sub>. The ratiometric images were generated by using special macros under ImageJ that divides the image of the  $I_{550-600}$  channel by that of the  $I_{600-650}$  channel. For each pixel, a pseudo-color scale is used for coding the ratio, while the intensity is defined by the integral intensity recorded for both channels at the corresponding pixel. Cholesterol extraction was induced by incubating the cells with 5 mM of Me- $\beta$ -cyclodextrine (MBCD) in reduced serum medium (Opti-MEM, Gibco Invitrogen) for 1h at 37°C with consecutive washing with fresh HBSS.<sup>79</sup> Cholesterol enrichment was induced by incubating the cells with a saturated complex of MBCD+Cholesterol (48 mg/g of Cholesterol) in reduced serum medium (Opti-MEM, Gibco Invitrogen) (total MBCD concentration was 5 mM) for 3h at 37°C followed by consecutive washing with fresh HBSS.<sup>69</sup> Oxidative stress was induced by incubating the cells with 2 mM solution of H<sub>2</sub>O<sub>2</sub> in HBSS for 1h at 37°C with consecutive washing with fresh HBSS.<sup>80</sup> In all cases microscopy imaging was started 70 minutes after the end of incubation with H<sub>2</sub>O<sub>2</sub>. Hyperosmotic stress was induced by replacing half of the cell medium with 1M sucrose solution immediately followed by imaging.<sup>5</sup>

## ASSOCIATED CONTENT

Supporting Information. Synthesis schemes for Nile Red probes for organelles. Spectroscopy data in LUVs. Colocalization microscopy images in KB and HeLa cells. Raw data and reconstructed ratiometric

microscopy images in live KB cells in various conditions. Tables: spectroscopy data in LUVs and organic solvents; Pearson's correlation coefficients for colocalization experiments; weighted arithmetic mean values obtained from ratiometric microscopy images in various conditions.

The Supporting Information is available free of charge at <https://pubs.acs.org/doi/>

## AUTHOR INFORMATION

Notes

\* Corresponding author: [andrey.klymchenko@unistra.fr](mailto:andrey.klymchenko@unistra.fr)

The authors declare no competing financial interest.

## ACKNOWLEDGMENTS

This work was supported by the European Research Council ERC Consolidator grant BrightSens 648528. D.D. was supported by a fellowship from the Ministère de la Recherche (France). Bohdan Wasylyk is acknowledged for providing the KB cells.

## REFERENCES

- (1) Zhu, H.; Fan, J.; Du, J.; Peng, X. Fluorescent Probes for Sensing and Imaging within Specific Cellular Organelles. *Acc. Chem. Res.* **2016**, *49*, 2115-2126.
- (2) Xu, W.; Zeng, Z.; Jiang, J. H.; Chang, Y. T.; Yuan, L. Discerning the Chemistry in Individual Organelles with Small-Molecule Fluorescent Probes. *Angew. Chem. Int. Ed.* **2016**, *55*, 13658-13699.
- (3) Srikun, D.; Albers, A. E.; Nam, C. I.; Iavaron, A. T.; Chang, C. J. Organelle-Targetable Fluorescent Probes for Imaging Hydrogen Peroxide in Living Cells Via Snap-Tag Protein Labeling. *J. Am. Chem. Soc.* **2010**, *132*, 4455-4465.
- (4) Gao, P.; Pan, W.; Li, N.; Tang, B. Fluorescent Probes for Organelle-Targeted Bioactive Species Imaging. *Chem. Sci.* **2019**, *10*, 6035-6071.
- (5) Goujon, A.; Colom, A.; Strakova, K.; Mercier, V.; Mahecic, D.; Manley, S.; Sakai, N.; Roux, A.; Matile, S. Mechanosensitive Fluorescent Probes to Image Membrane Tension in Mitochondria, Endoplasmic Reticulum, and Lysosomes. *J. Am. Chem. Soc.* **2019**, *141*, 3380-3384.
- (6) Hu, F.; Liu, B. Organelle-Specific Bioprobes Based on Fluorogens with Aggregation-Induced Emission (Aie) Characteristics. *Org. Biomol. Chem.* **2016**, *14*, 9931-9944.
- (7) Cerrato, C. P.; Kunnappu, K.; Langel, U. Cell-Penetrating Peptides with Intracellular Organelle Targeting. *Expert Opin. Drug Deliv.* **2017**, *14*, 245-255.
- (8) Lukinavicius, G.; Reymond, L.; Umezawa, K.; Sallin, O.; D'Este, E.; Gottfert, F.; Ta, H.; Hell, S. W.; Urano, Y.; Johnsson, K. Fluorogenic Probes for Multicolor Imaging in Living Cells. *Journal of the American Chemical Society* **2016**, *138*, 9365-9368.
- (9) Lingwood, D.; Simons, K. Lipid Rafts as a Membrane-Organizing Principle. *Science* **2010**, *327*, 46-50.
- (10) Sezgin, E.; Levental, I.; Mayor, S.; Eggeling, C. The Mystery of Membrane Organization: Composition, Regulation and Roles of Lipid Rafts. *Nat. Rev. Mol. Cell Biol.* **2017**, *18*, 361-374.
- (11) Martin, S.; Parton, R. G. Lipid Droplets: A Unified View of a Dynamic Organelle. *Nat. Rev. Mol. Cell Biol.* **2006**, *7*, 373-378.

- (12) Mesmin, B.; Maxfield, F. R. Intracellular Sterol Dynamics. *Biochim. Biophys. Acta Mol. Cell Biol. Lipids* **2009**, *1791*, 636-645.
- (13) Ikonen, E. Cellular Cholesterol Trafficking and Compartmentalization. *Nat. Rev. Mol. Cell Biol.* **2008**, *9*, 125-138.
- (14) Brown, D. A.; London, E. Structure and Function of Sphingolipid- and Cholesterol-Rich Membrane Rafts. *J. Biol. Chem.* **2000**, *275*, 17221-17224.
- (15) Stone, M. B.; Shelby, S. A.; Veatch, S. L. Super-Resolution Microscopy: Shedding Light on the Cellular Plasma Membrane. *Chem. Rev.* **2017**, *117*, 7457-7477.
- (16) Risselada, H. J.; Marrink, S. J. The Molecular Face of Lipid Rafts in Model Membranes. *Proc. Natl. Acad. Sci. U. S. A.* **2008**, *105*, 17367-17372.
- (17) Levental, K. R.; Malmberg, E.; Symons, J. L.; Fan, Y. Y.; Chapkin, R. S.; Ernst, R.; Levental, I. Lipidomic and Biophysical Homeostasis of Mammalian Membranes Counteracts Dietary Lipid Perturbations to Maintain Cellular Fitness. *Nature Communications* **2020**, *11*, 13.
- (18) Aguilar, P. S.; de Mendoza, D. Control of Fatty Acid Desaturation: A Mechanism Conserved from Bacteria to Humans. *Mol. Microbiol.* **2006**, *62*, 1507-1514.
- (19) Shyu, P.; Wong, X. F. A.; Crasta, K.; Thibault, G. Dropping in on Lipid Droplets: Insights into Cellular Stress and Cancer. *Biosci. Rep.* **2018**, *38*, BSR20180764.
- (20) Vyšniauskas, A.; Kuimova, M. K. A Twisted Tale: Measuring Viscosity and Temperature of Microenvironments Using Molecular Rotors. *Int. Rev. Phys. Chem.* **2018**, *37*, 259-285.
- (21) Klymchenko, A. S. Solvatochromic and Fluorogenic Dyes as Environment-Sensitive Probes: Design and Biological Applications. *Acc. Chem. Res.* **2017**, *50*, 366-375.
- (22) Su, D.; Teoh, C. L.; Wang, L.; Liu, X.; Chang, Y. T. Motion-Induced Change in Emission (Mice) for Developing Fluorescent Probes. *Chem. Soc. Rev.* **2017**, *46*, 4833-4844.
- (23) Haidekker, M. A.; Theodorakis, E. A. Ratiometric Mechanosensitive Fluorescent Dyes: Design and Applications. *J. Mater. Chem. C Mater.* **2016**, *4*, 2707-2718.
- (24) Dent, M. R.; Lopez-Duarte, I.; Dickson, C. J.; Geoghegan, N. D.; Cooper, J. M.; Gould, I. R.; Krams, R.; Bull, J. A.; Brooks, N. J.; Kuimova, M. K. Imaging Phase Separation in Model Lipid Membranes through the Use of Bodipy Based Molecular Rotors. *Phys. Chem. Chem. Phys.* **2015**, *17*, 18393-18402.
- (25) Chambers, J. E.; Kubankova, M.; Huber, R. G.; Lopez-Duarte, I.; Avezov, E.; Bond, P. J.; Marciniak, S. J.; Kuimova, M. K. An Optical Technique for Mapping Microviscosity Dynamics in Cellular Organelles. *ACS Nano* **2018**, *12*, 4398-4407.
- (26) Humeniuk, H. V.; Rosspeintner, A.; Licari, G.; Kilin, V.; Bonacina, L.; Vauthey, E.; Sakai, N.; Matile, S. White-Fluorescent Dual-Emission Mechanosensitive Membrane Probes That Function by Bending Rather Than Twisting. *Angew. Chem. Int. Ed.* **2018**, *57*, 10559-10563.
- (27) Dal Molin, M.; Verole, Q.; Colom, A.; Letrun, R.; Derivery, E.; Gonzalez-Gaitan, M.; Vauthey, E.; Roux, A.; Sakai, N.; Matile, S. Fluorescent Flippers for Mechanosensitive Membrane Probes. *J. Am. Chem. Soc.* **2015**, *137*, 568-571.
- (28) Mercier, V.; Larios, J.; Molinard, G.; Goujon, A.; Matile, S.; Gruenberg, J.; Roux, A. Endosomal Membrane Tension Regulates Escrt-Iii-Dependent Intra-Lumenal Vesicle Formation. *Nat. Cell Biol.* **2020**, *22*, 947-959.
- (29) Colom, A.; Derivery, E.; Soleimanpour, S.; Tomba, C.; Molin, M. D.; Sakai, N.; Gonzalez-Gaitan, M.; Matile, S.; Roux, A. A Fluorescent Membrane Tension Probe. *Nat. Chem.* **2018**, *10*, 1118-1125.
- (30) Straková, K.; López-Andarias, J.; Jiménez-Rojo, N.; Chambers, J. E.; Marciniak, S. J.; Riezman, H.; Sakai, N.; Matile, S. Haloflippers: A General Tool for the Fluorescence Imaging of Precisely Localized Membrane Tension Changes in Living Cells. *ACS Cent. Sci.* **2020**, *6*, 1376-1385.
- (31) Klymchenko, A. S.; Kreder, R. Fluorescent Probes for Lipid Rafts: From Model Membranes to Living Cells. *Chem. Biol.* **2014**, *21*, 97-113.
- (32) Liu, C.; Tian, M.; Lin, W. A Unique Polarity-Sensitive Photothermal Sensitizer Revealing Down-Regulated Mitochondrial Polarity During Photo-Induced Cell Death. *J. Mater. Chem. B* **2020**, *8*, 752-757.

- (33) Shynkar, V. V.; Klymchenko, A. S.; Kunzelmann, C.; Duportail, G.; Muller, C. D.; Demchenko, A. P.; Freyssinet, J. M.; Mely, Y. Fluorescent Biomembrane Probe for Ratiometric Detection of Apoptosis. *J. Am. Chem. Soc.* **2007**, *129*, 2187-2193.
- (34) Ashoka, A. H.; Ashokkumar, P.; Kovtun, Y. P.; Klymchenko, A. S. Solvatochromic near-Infrared Probe for Polarity Mapping of Biomembranes and Lipid Droplets in Cells under Stress. *J. Phys. Chem. Lett.* **2019**, *10*, 2414-2421.
- (35) Ghosh, S.; Nandi, S.; Ghosh, C.; Bhattacharyya, K. Fluorescence Dynamics in the Endoplasmic Reticulum of a Live Cell: Time-Resolved Confocal Microscopy. *ChemPhysChem* **2016**, *17*, 2818-2823.
- (36) Jiang, N.; Fan, J.; Xu, F.; Peng, X.; Mu, H.; Wang, J.; Xiong, X. Ratiometric Fluorescence Imaging of Cellular Polarity: Decrease in Mitochondrial Polarity in Cancer Cells. *Angew. Chem. Int. Ed.* **2015**, *54*, 2510-2514.
- (37) Amaro, M.; Reina, F.; Hof, M.; Eggeling, C.; Sezgin, E. Laurdan and Di-4-Anepdhq Probe Different Properties of the Membrane. *J. Phys. D Appl. Phys.* **2017**, *50*, 134004.
- (38) Zhang, Y. L.; Frangos, J. A.; Chachisvilis, M. Laurdan Fluorescence Senses Mechanical Strain in the Lipid Bilayer Membrane. *Biochem. Biophys. Res. Commun.* **2006**, *347*, 838-841.
- (39) Dietrich, C.; Bagatolli, L. A.; Volovyk, Z. N.; Thompson, N. L.; Levi, M.; Jacobson, K.; Gratton, E. Lipid Rafts Reconstituted in Model Membranes. *Biophys. J.* **2001**, *80*, 1417-1428.
- (40) Jin, L.; Millard, A. C.; Wuskell, J. P.; Dong, X. M.; Wu, D. Q.; Clark, H. A.; Loew, L. M. Characterization and Application of a New Optical Probe for Membrane Lipid Domains. *Biophys. J.* **2006**, *90*, 2563-2575.
- (41) Kwiatek, J. M.; Owen, D. M.; Abu-Siniyeh, A.; Yan, P.; Loew, L. M.; Gaus, K. Characterization of a New Series of Fluorescent Probes for Imaging Membrane Order. *Plos One* **2013**, *8*, e52960.
- (42) Oncul, S.; Klymchenko, A. S.; Kucherak, O. A.; Demchenko, A. P.; Martin, S.; Dontenwill, M.; Arntz, Y.; Didier, P.; Duportail, G.; Mely, Y. Liquid Ordered Phase in Cell Membranes Evidenced by a Hydration-Sensitive Probe: Effects of Cholesterol Depletion and Apoptosis. *Biochim. Biophys. Acta Biomembr.* **2010**, *1798*, 1436-1443.
- (43) Kucherak, O. A.; Oncul, S.; Darwich, Z.; Yushchenko, D. A.; Arntz, Y.; Didier, P.; Mely, Y.; Klymchenko, A. S. Switchable Nile Red-Based Probe for Cholesterol and Lipid Order at the Outer Leaflet of Biomembranes. *J. Am. Chem. Soc.* **2010**, *132*, 4907-4916.
- (44) Castro-Castillo, V.; Gajardo, J.; Sandoval-Altamirano, C.; Gratton, E.; Sanchez, S.; Malacrida, L.; Gunther, G. Caprydaa, an Anthracene Dye Analog to Laurdan: A Comparative Study Using Cuvette and Microscopy. *J. Mater. Chem. B* **2020**, *8*, 88-99.
- (45) Valanciunaite, J.; Kempf, E.; Seki, H.; Danylchuk, D. I.; Peyrieras, N.; Niko, Y.; Klymchenko, A. S. Polarity Mapping of Cells and Embryos by Improved Fluorescent Solvatochromic Pyrene Probe. *Anal. Chem.* **2020**, *92*, 6512-6520.
- (46) Niko, Y.; Didier, P.; Mely, Y.; Konishi, G.; Klymchenko, A. S. Bright and Photostable Push-Pull Pyrene Dye Visualizes Lipid Order Variation between Plasma and Intracellular Membranes. *Sci. Rep.* **2016**, *6*, 18870.
- (47) Kim, H. M.; Choo, H.-J.; Jung, S.-Y.; Ko, Y.-G.; Park, W.-H.; Jeon, S.-J.; Kim, C. H.; Joo, T.; Cho, B. R. A Two-Photon Fluorescent Probe for Lipid Raft Imaging: C-Laurdan. *ChemBioChem* **2007**, *8*, 553-559.
- (48) Danylchuk, D. I.; Sezgin, E.; Chabert, P.; Klymchenko, A. S. Redesigning Solvatochromic Probe Laurdan for Imaging Lipid Order Selectively in Cell Plasma Membranes. *Anal. Chem.* **2020**, *92*, 14798-14805.
- (49) Owen, D. M.; Rentero, C.; Magenau, A.; Abu-Siniyeh, A.; Gaus, K. Quantitative Imaging of Membrane Lipid Order in Cells and Organisms. *Nat. Protoc.* **2012**, *7*, 24-35.
- (50) Jimenez-Sanchez, A.; Lei, E. K.; Kelley, S. O. A Multifunctional Chemical Probe for the Measurement of Local Micropolarity and Microviscosity in Mitochondria. *Angew. Chem. Int. Ed.* **2018**, *57*, 8891-8895.
- (51) Iaea, D. B.; Maxfield, F. R. Membrane Order in the Plasma Membrane and Endocytic Recycling Compartment. *PLoS One* **2017**, *12*, e0188041.

- (52) Li, L. L.; Li, K.; Li, M. Y.; Shi, L.; Liu, Y. H.; Zhang, H.; Pan, S. L.; Wang, N.; Zhou, Q.; Yu, X. Q. Bodipy-Based Two-Photon Fluorescent Probe for Real-Time Monitoring of Lysosomal Viscosity with Fluorescence Lifetime Imaging Microscopy. *Anal. Chem.* **2018**, *90*, 5873-5878.
- (53) Guo, R.; Yin, J.; Ma, Y.; Wang, Q.; Lin, W. A Novel Mitochondria-Targeted Rhodamine Analogue for the Detection of Viscosity Changes in Living Cells, Zebra Fish and Living Mice. *J. Mater. Chem. B* **2018**, *6*, 2894-2900.
- (54) Palacios-Serrato, E.; Araiza-Olivera, D.; Jiménez-Sánchez, A. Fluorescent Probe for Transmembrane Dynamics During Osmotic Effects. *Anal. Chem.* **2020**, *92*, 3888-3895.
- (55) Greenspan, P.; Mayer, E. P.; Fowler, S. D. Nile Red - a Selective Fluorescent Stain for Intracellular Lipid Droplets. *J. Cell Biol.* **1985**, *100*, 965-973.
- (56) Bongiovanni, M. N.; Godet, J.; Horrocks, M. H.; Tosatto, L.; Carr, A. R.; Wirthensohn, D. C.; Ranasinghe, R. T.; Lee, J. E.; Ponjavic, A.; Fritz, J. V.; Dobson, C. M.; Klenerman, D.; Lee, S. F. Multi-Dimensional Super-Resolution Imaging Enables Surface Hydrophobicity Mapping. *Nat. Commun.* **2016**, *7*, 9.
- (57) Wang, H. M.; Feng, Z. Q. Q.; Del Signore, S. J.; Rodal, A. A.; Xu, B. Active Probes for Imaging Membrane Dynamics of Live Cells with High Spatial and Temporal Resolution over Extended Time Scales and Areas. *J. Am. Chem. Soc.* **2018**, *140*, 3505-3509.
- (58) Danylchuk, D. I.; Moon, S.; Xu, K.; Klymchenko, A. S. Switchable Solvatochromic Probes for Live-Cell Super-Resolution Imaging of Plasma Membrane Organization. *Angew. Chem. Int. Ed.* **2019**, *58*, 14920-14924.
- (59) Zielonka, J.; Joseph, J.; Sikora, A.; Hardy, M.; Ouari, O.; Vasquez-Vivar, J.; Cheng, G.; Lopez, M.; Kalyanaraman, B. Mitochondria-Targeted Triphenylphosphonium-Based Compounds: Syntheses, Mechanisms of Action, and Therapeutic and Diagnostic Applications. *Chem. Rev.* **2017**, *117*, 10043-10120.
- (60) Wagner, N.; Stephan, M.; Hoglinger, D.; Nadler, A. A Click Cage: Organelle-Specific Uncaging of Lipid Messengers. *Angew. Chem. Int. Ed.* **2018**, *57*, 13339-13343.
- (61) Yang, Z.; He, Y.; Lee, J. H.; Park, N.; Suh, M.; Chae, W. S.; Cao, J.; Peng, X.; Jung, H.; Kang, C.; Kim, J. S. A Self-Calibrating Bipartite Viscosity Sensor for Mitochondria. *J. Am. Chem. Soc.* **2013**, *135*, 9181-9185.
- (62) Kong, X.; Yin, J.; Li, M.; Zhu, L.; Dong, B.; Ma, Y.; Lin, W. Simultaneously Imaging of So<sub>2</sub> in Lysosomes and Mitochondria Based on a Dual Organelle-Targeted Fluorescent Probe. *Sens. Actuators B Chem.* **2019**, *292*, 80-87.
- (63) Zhang, H.; Fan, J.; Dong, H.; Zhang, S.; Xu, W.; Wang, J.; Gao, P.; Peng, X. Fluorene-Derived Two-Photon Fluorescent Probes for Specific and Simultaneous Bioimaging of Endoplasmic Reticulum and Lysosomes: Group-Effect and Localization. *J. Mater. Chem. B* **2013**, *1*, 5450-5455.
- (64) Hirayama, T.; Inden, M.; Tsuboi, H.; Niwa, M.; Uchida, Y.; Naka, Y.; Hozumi, I.; Nagasawa, H. A Golgi-Targeting Fluorescent Probe for Labile Fe(II) to Reveal an Abnormal Cellular Iron Distribution Induced by Dysfunction of Vps35. *Chem. Sci.* **2019**, *10*, 1514-1521.
- (65) Collot, M.; Fam, T. K.; Ashokkumar, P.; Faklaris, O.; Galli, T.; Danglot, L.; Klymchenko, A. S. Ultrabright and Fluorogenic Probes for Multicolor Imaging and Tracking of Lipid Droplets in Cells and Tissues. *J. Am. Chem. Soc.* **2018**, *140*, 5401-5411.
- (66) Steinkuhler, J.; Sezgin, E.; Urbancic, I.; Eggeling, C.; Dimova, R. Mechanical Properties of Plasma Membrane Vesicles Correlate with Lipid Order, Viscosity and Cell Density. *Commun. Biol.* **2019**, *2*, 337.
- (67) Tabas, I. Consequences of Cellular Cholesterol Accumulation: Basic Concepts and Physiological Implications. *J. Clin. Invest.* **2002**, *110*, 905-911.
- (68) Carstea, E. D.; Morris, J. A.; Coleman, K. G.; Loftus, S. K.; Zhang, D.; Cummings, C.; Gu, J.; Rosenfeld, M. A.; Pavan, W. J.; Krizman, D. B.; Nagle, J.; Polymeropoulos, M. H.; Sturley, S. L.; Ioannou, Y. A.; Higgins, M. E.; Comly, M.; Cooney, A.; Brown, A.; Kaneski, C. R.; Blanchette-Mackie, E. J.; Dwyer, N. K.; Neufeld, E. B.; Chang, T. Y.; Liscum, L.; Strauss, J. F.; Ohno, K.; Zeigler, M.; Carmi, R.; Sokol, J.; Markie, D.; Oneill, R. R.; vanDiggelen, O. P.; Elleder, M.; Patterson, M. C.; Brady,

- R. O.; Vanier, M. T.; Pentchev, P. G.; Tagle, D. A. Niemann-Pick C1 Disease Gene: Homology to Mediators of Cholesterol Homeostasis. *Science* **1997**, *277*, 228-231.
- (69) Zidovetzki, R.; Levitan, I. Use of Cyclodextrins to Manipulate Plasma Membrane Cholesterol Content: Evidence, Misconceptions and Control Strategies. *Biochim. Biophys. Acta-Biomembr.* **2007**, *1768*, 1311-1324.
- (70) Yin, H.; Xu, L.; Porter, N. A. Free Radical Lipid Peroxidation: Mechanisms and Analysis. *Chem. Rev.* **2011**, *111*, 5944-5972.
- (71) Nilsson, E.; Ghassemifar, R.; Brunk, U. T. Lysosomal Heterogeneity between and within Cells with Respect to Resistance against Oxidative Stress. *Histochem. J.* **1997**, *29*, 857-865.
- (72) Lenaz, G. Role of Mitochondria in Oxidative Stress and Ageing. *Biochim. Biophys. Acta Bioenerg.* **1998**, *1366*, 53-67.
- (73) Ott, M.; Gogvadze, V.; Orrenius, S.; Zhivotovsky, B. Mitochondria, Oxidative Stress and Cell Death. *Apoptosis* **2007**, *12*, 913-922.
- (74) Mammoto, T.; Mammoto, A.; Ingber, D. E. In *Annu. Rev. Cell Dev. Biol.*; Schekman, R., Ed.; Annual Reviews: Palo Alto, 2013; Vol. 29, p 27-61.
- (75) Ladoux, B.; Mege, R. M. Mechanobiology of Collective Cell Behaviours. *Nat. Rev. Mol. Cell Biol.* **2017**, *18*, 743-757.
- (76) Chaudhuri, P. K.; Low, B. C.; Lim, C. T. Mechanobiology of Tumor Growth. *Chem. Rev.* **2018**, *118*, 6499-6515.
- (77) Alam Shibly, S. U.; Ghatak, C.; Sayem Karal, M. A.; Moniruzzaman, M.; Yamazaki, M. Experimental Estimation of Membrane Tension Induced by Osmotic Pressure. *Biophys. J.* **2016**, *111*, 2190-2201.
- (78) Deda, M. L.; Ghedini, M.; Aiello, I.; Pugliese, T.; Barigelletti, F.; Accorsi, G. Organometallic Emitting Dyes: Palladium(II) Nile Red Complexes. *Journal of Organometallic Chemistry* **2005**, *690*, 857-861.
- (79) Onodera, R.; Motoyama, K.; Okamoto, A.; Higashi, T.; Kariya, R.; Okada, S.; Arima, H. Involvement of Cholesterol Depletion from Lipid Rafts in Apoptosis Induced by Methyl-B-Cyclodextrin. *Int J Pharm* **2013**, *452*, 116-123.
- (80) de la Haba, C.; Palacio, J. R.; Martinez, P.; Morros, A. Effect of Oxidative Stress on Plasma Membrane Fluidity of Thp-1 Induced Macrophages. *Biochim Biophys Acta* **2013**, *1828*, 357-364.

## TOC GRAPHIC

